

AN *IUE* ATLAS OF PRE-MAIN-SEQUENCE STARS. III. CO-ADDED FINAL ARCHIVE SPECTRA FROM THE LONG-WAVELENGTH CAMERAS

JEFF A. VALENTI

Space Telescope Science Institute, 3700 San Martin Drive, Baltimore, MD 21218; valenti@stsci.edu

ADAM A. FALLON¹

Department of Physics and Astronomy, Macalester College, 1600 Grand Avenue, Saint Paul, MN 55015; afallon@astro.columbia.edu

AND

CHRISTOPHER M. JOHNS-KRULL

Department of Physics and Astronomy, Rice University, 6100 Main Street, MS-108, Houston, TX 77005; cmj@rice.edu

Received 2002 October 8; accepted 2003 March 14

ABSTRACT

We identified 137 T Tauri stars (TTS) and 97 Herbig Ae/Be (HAEBE) stars observed by *IUE* in the wavelength interval 1900–3200 Å. Each low-resolution ($R \sim 6$ Å) spectrum was visually inspected for source contamination and data quality, and then all usable spectra were combined to form a single time averaged spectrum for each star. For sources with multiple observations, we characterized variability and compared with previously published amplitudes at shorter wavelengths. We combined several co-added spectra of diskless TTS to produce a pair of intrinsic stellar spectra unaffected by accretion. We then fitted spectra of TTS with the reddened sum of an intrinsic spectrum and a schematic veiling continuum, measuring emission line fluxes from the residuals. We used extinction and distance estimates from the literature to convert measured Mg II line fluxes into intrinsic line luminosities, noting that the *IUE* detection limit introduces a sample bias such that intrinsic line luminosity is correlated with extinction. This sample bias complicates any physical interpretation of TTS intrinsic luminosities. We measured extinction toward HAEBE stars by fitting our co-added *IUE* spectra with reddened spectra of main-sequence stars and also from V band minus 3000 Å color excess. We measured excess line emission and absorption in spectra of HAEBE stars divided by fitted spectra of main-sequence stars, noting that HAEBE stars with an infrared excess indicating circumstellar material typically also have anomalous UV line strengths. In the latter situation, Mg II is usually shallower than in a main-sequence star of the same spectral class, whereas Fe II lines are equally likely to be deeper or shallower. Our co-added spectra of TTS, HAEBE stars, and main-sequence templates are available electronically.

Subject headings: accretion, accretion disks — atlases — stars: pre-main-sequence — ultraviolet: stars

On-line material: machine-readable tables

1. INTRODUCTION

1.1. *IUE* Data

Although the *International Ultraviolet Explorer* (*IUE*) satellite ceased operations on 1996 September 27, the vast archive of *IUE* spectra continues to be an important astronomical resource. Ultraviolet (UV) spectrographs on the *Hubble Space Telescope* (*HST*) have observed only a small fraction of the pre-main-sequence (PMS) stars observed by *IUE*. Historically, the first dedicated *IUE* spectral atlas of PMS stars was published by Gómez de Castro & Franqueira (1997), who also tabulated selected line fluxes without uncertainties. Valenti, Johns-Krull, & Linsky (2000, hereafter Paper I) constructed a low-resolution spectral atlas and catalog of line fluxes for short-wavelength (1150–1980 Å) *IUE* spectra of PMS stars. Johns-Krull, Valenti, & Linsky (2000, hereafter Paper II) used these line fluxes to investigate the effects of accretion and magnetic activity on short-wavelength spectra of T Tauri stars (TTS). Here we extend our earlier work to low-resolution spectra in the long-wavelength bandpass of *IUE*.

The *IUE* final archive project (Nichols & Linsky 1996) provided the original technical motivation for constructing a catalog of *IUE* observations of PMS stars. Final archive reprocessing with NEWSIPS (rather than the original IUESIPS) software (described in detail by Nichols et al. 1994) generally improved signal-to-noise (S/N) ratios and reduced fixed-pattern noise, especially for noisy spectra. Wavelength and photometric accuracy were also improved significantly.

The signal-weighted extraction algorithm in NEWSIPS attempted to determine empirically the cross-dispersion profile and the spectrum location. When both of these operations failed and default values were assumed, NEWSIPS sometimes yielded anomalously low emission line fluxes. To overcome this problem, the *IUE* Newly Extracted Spectra (INES) package uses a different algorithm to extract spectra from the two-dimensional images created by NEWSIPS (Rodríguez-Pascual et al. 1999). NEWSIPS extracted spectra are adequate for our project because NEWSIPS assumed default profiles and locations for only 10% of the 1062 images. The NEWSIPS assumptions are correct for some fraction of these cases, and for noisy images the distinction is not significant. Aside from this issue, Huélamo, Franqueira, & Gómez de Castro (2000) find that the two packages agree to within their uncertainty estimates. On the other hand, Massa & Fitzpatrick (2000) argue

¹ Currently at Department of Astronomy, Columbia University, 550 West 120th Street, New York, NY 10027.

that NEWSIPS fluxes can have errors of 10%–15%. These calibration errors can be reduced somewhat by co-adding spectra from different epochs.

The *IUE* long-wavelength prime and redundant (LWP and LWR) cameras obtained useful spectra in the wavelength interval 1900–3200 Å. In this bandpass the most prominent spectral features are the Mg II resonance doublet at 2800 Å and numerous low-excitation Fe II lines. *IUE* long-wavelength (LW) data are of particular interest in the study of PMS stars because useful spectra exist for 86 sources that were not observed in the short-wavelength (SW) bandpass of *IUE*. In addition, observed continua are stronger at longer wavelengths, allowing a more detailed analysis of emission and absorption features than was possible with the SW data presented in Paper I. Finally, for 113 stars with usable spectra both here and in Paper I, co-added spectra now cover the entire *IUE* bandpass from 1150–3200 Å.

In Paper I, the enhanced data quality in the *IUE* final archive permitted identification of H₂ fluorescent emission in spectra of 12 TTS and measurement of extinction and circumstellar absorption around higher mass PMS stars. These results illustrate how a large sample of UV spectra can facilitate the study of young stars and their environments. This extension of our PMS catalog to the LW bandpass of *IUE* explores new extinction and spectral line diagnostics.

1.2. T Tauri Stars

TTS are low-mass ($M \lesssim 2 M_{\odot}$) PMS stars that are optically visible, as reviewed by Bertout (1989). TTS were originally divided into two observationally defined classes, with classical TTS (CTTS) having larger H α equivalent widths than weak TTS. Alternatively, TTS can be distinguished by whether or not material is accreting from a disk onto the stellar surface. In this more physical classification scheme, CTTS are accreting, whereas naked TTS (NTTS) are not (Walter 1986). Directly or indirectly, most excess emission from CTTS can be attributed to the presence of a disk interacting with a magnetically active star. Some weak TTS are accreting, yet still have relatively small H α equivalent widths, making the original classification scheme potentially confusing. We therefore adopt the more physical nomenclature, using CTTS and NTTS to distinguish whether or not TTS are accreting. FU Ori stars (see review by Hartmann & Kenyon 1996) are CTTS in outburst, accreting material at a rate $\sim 10^3$ times greater than a typical CTTS.

The presence of a disk and accretion of material onto the surface of CTTS gives rise to excess continuum emission that veils stellar spectra, reducing the depths of photospheric absorption lines. Veiling is observable at *IUE*, optical, and infrared (IR) wavelengths (e.g., Herbig & Goodrich 1986; Basri & Batalha 1990; Paper II; Johns-Krull & Valenti 2001). Magnetospheric accretion models (Uchida & Shibata 1984; Bertout, Basri, & Bouvier 1988; Camenzind 1990; Königl 1991; Shu et al. 1994; Paatz & Camenzind 1996) invoke strong stellar magnetic fields that truncate the disk at several stellar radii, redirecting disk material along magnetic field lines to accretion footprints on the stellar surface. Material impacts the surface at close to free-fall speeds, producing excess continuum emission in a strong shock (Calvet & Gullbring 1998). This shock also produces line emission in the UV

(Lamzin 1995, 1998; Paper II; Ardila et al. 2002), making *IUE* data particularly relevant for studying accretion onto CTTS. Magnetic activity on TTS also produces observable signatures in the UV that can be difficult to distinguish from accretion (Paper II).

Finally, CTTS systems lose mass at rates sufficient to produce significant blueshifted absorption in strong resonance lines, such as the Mg II doublet near 2800 Å (see Imhoff & Appenzeller 1987). The long-wavelength bandpass of *IUE* contains numerous Fe II lines that have generally been ignored in studies of CTTS outflows. High-resolution spectra of these Fe II lines have been used to study winds from cool giants (e.g., Carpenter et al. 1999), but even low-resolution *IUE* spectra permit an initial investigation of CTTS outflows.

1.3. Herbig Ae/Be Stars

Herbig Ae/Be (HAEBE) stars are conceptually defined as high-mass analogs of TTS, but it can be difficult to establish observationally the youth of a candidate HAEBE star (see review by Waters & Waelkens 1998). By analogy to CTTS, candidate HAEBE stars are often identified by the presence of an IR excess (e.g., Thé, de Winter, & Pérez 1994). IR colors of some HAEBE stars suggest the presence of circumstellar material that is not confined to a disk (Hillenbrand et al. 1992; Hartmann, Kenyon, & Calvet 1993). Nevertheless, it is widely believed that HAEBE stars have disks and actively accrete in a manner similar to CTTS. Testing this hypothesis is a key goal of current studies of HAEBE stars. Malfait, Bogaert, & Waelkens (1998) suggest that as HAEBE stars evolve, circumstellar properties change.

In four HAEBE stars of late spectral type, Blondel & Djie (1994) report a UV continuum excess that they attribute to accretion. Meeus, Waelkens, & Malfait (1998) obtain a similar result for three late A-type HAEBE stars. On the other hand, detailed searches for veiling in several HAEBE stars of earlier spectral type have produced negative results (Böhm & Catala 1993; Ghadour et al. 1994). Detection of excess continuum in hot HAEBE stars is difficult because shallow photospheric lines poorly constrain direct veiling measurements, especially at low resolution. Also, extinction and veiling can have similar effects on continuum slope, though the 2200 Å bump helps lift the degeneracy. A systematic analysis of *IUE* spectra of HAEBE stars may provide more evidence for a continuum excess due to accretion. In addition, HAEBE stars also have strong winds that can be analyzed using UV diagnostics (e.g., Bouret & Catala 1998).

In § 2 we define our sample of PMS stars and describe our procedure for assessing and combining spectra. We then present the atlas of co-added *IUE* spectra, providing quantitative indicators of source variability. In § 3 we fit each co-added CTTS spectra with an NTTS template plus a polynomial approximation to the veiling continuum. We then measure emission line fluxes above the fitted model. We also determine extinction toward HAEBE stars by fitting co-added spectra with main-sequence templates. We then measure excess line emission, relative to the fitted templates. Finally, in § 4 we discuss the atlas and our measurements based on the atlas, highlighting opportunities for future investigation.

2. ATLAS OF SPECTRA

2.1. Sample Selection

Following the methodology of Paper I, we identified all LWP or LWR exposures obtained with a nominal *IUE* pointing within 2' of a known or candidate PMS star. This search radius accommodates the likely range of coordinate errors in NEWSIPS headers. We compared positions from the headers with coordinates for PMS stars in Herbig & Bell (1988), Hillenbrand (1997), Feigelson et al. (1993), Thé et al. (1994), Walter et al. (1994), and the SIMBAD database (object types pr*, TT*, Or*, or FU*). The coordinate matching procedure yielded 238 sources potentially observed by *IUE* in the LW bandpass. It is possible that we have missed a few PMS stars due to coordinate errors.

Table 1 lists in order of right ascension 238 known or candidate PMS stars for which coordinate matching indicates at least one possible LW observation by *IUE*. For reference within this paper, we assign each source an identification number between 1 and 238, but future citations should use standard nomenclature to refer to individual objects. For sources that also appear in Paper I, the identification number from Paper I appears in column (2) of Table 1. Column (3) lists the Herbig & Bell (1988) catalog number, if applicable. Alternate source names are given in column (4) and column (5) with catalog precedence as described in the table note. Column (6) gives spectral types taken preferentially from Paper I, Herbig & Bell (1988), Thé et al. (1994), and then other source material used in defining the sample. We present these spectral types without comment as to their veracity. In § 3.4 we use template fitting to determine alternate spectral types for some HAEBE stars. Column (8) gives the number of *IUE* spectra combined to produce each atlas spectrum, after manually rejecting unsuitable spectra. Sources with no usable spectra are retained in Table 1 to flag the existence of unusable data.

Column (7) of Table 1 classifies each source as a HAEBE star, CTTS, NTTS, FU Ori object (FUOri), or non-PMS star (nonPMS). The four non-PMS stars erroneously appear in PMS source catalogs. We retain them in Table 1 for reference, but they are not considered in the subsequent analysis. For the TTS listed by name and identification number in Table 2, the PMS catalogs used to select our sample did not indicate accretion status. We adopt a CTTS or NTTS classification for these stars based on published indications of near-IR (NIR) excess, large H α equivalent width (EW), broad H α emission profiles, or redshifted absorption components. Table 2 lists our adopted PMS categorizations, reasons for the assignment, and supporting literature citations. In some cases, our classifications are subjective and subject to change.

2.2. Combining Spectra

Our search of the *IUE* merged log yielded camera sequence numbers (e.g., lwp02061) for 1062 LW images of 238 PMS stars. Some images contain two adjacent spectra, obtained by exposing once with the source in the large aperture and once in the small aperture prior to a single read of the detector. As a result, the 1062 images actually contain 1224 spectra. Using the Multi-Mission Archive at Space Telescope (MAST), we successfully retrieved 1060 images containing 1222 spectra (a 99.8% success rate). In Paper I our retrieval success rate for SW images was only 91%.

Either final archive processing of SW images was incomplete in 1996 October (Paper I), or perhaps final archive processing fails on a larger fraction of images in the SW bandpass.

As in Paper I, an interactive procedure was used to assess whether each individual spectrum warranted inclusion in the final weighted mean spectrum. Individual spectra were overplotted with the mean spectrum superposed. For sources with many observations, individual spectra were examined successively in groups of six. Spectra were excluded from the mean for a variety of reasons recorded in the Appendix. Common reasons for rejecting spectra included no significant signal, relatively noisy spectrum, anomalously low flux, questionable spectral features, a preponderance of bad pixels ($>10\%$ with ν flags ≤ -8 , indicating a wide range of serious data problems), or indications of trouble noted in the NEWSIPS header. Table 3 of Paper I lists the FITS header fields that were inspected and nominal acceptance criteria that we adopted from chapter 13 of Garhart et al. (1997). Occasionally, we retained a spectrum that failed one or more acceptance tests, if the spectrum appeared better than all other spectra of the source. Such instances are noted in the Appendix.

Low-resolution *IUE* spectra have dispersions of 2.663, 2.666, and 2.669 Å pixel $^{-1}$ for the LWP, LWR(A), and LWR(B) cameras, where "A" and "B" refer to the intensity transfer functions (ITF) used when processing images (Garhart et al. 1997). For sources with useful spectra at only one dispersion, no interpolation was necessary. For sources with useful spectra at two or three dispersions, we linearly interpolated flux spectra onto the lowest-dispersion wavelength scale for that source [LWP, if present, and otherwise LWR(A)]. We determined uncertainties for the interpolated flux points by propagating the original uncertainties for each pixel. Note that when the new and old wavelength scales are significantly out of phase, linear interpolation effectively smooths the result, increasing the signal-to-noise (S/N) ratio and decreasing spectral resolution. For LWR spectra, we ignored the negligible difference in dispersion (<0.0004 Å pixel $^{-1}$) before and after 1980.1 and 1979.9 for ITF A and B, respectively. We did not attempt to align spectral features before co-addition because our main interest is line fluxes. Small residual errors in wavelength calibration will degrade spectral resolution in co-added spectra.

After wavelength interpolation, we renormalized individual spectra to match the unweighted mean flux for all spectra of a source in the wavelength range 1900–3200 Å, ignoring any bad pixels. We applied the same scale factor to the corresponding flux uncertainty vectors. This renormalization procedure removes intrinsic flux variations that would bias the weighted mean in favor of weaker spectra, which have lower uncertainties despite a worse S/N ratio. In Paper I, this effect was noted but ignored. After renormalization, we constructed a weighted mean flux spectrum for each source, weighting individual spectra by the inverse square of the corresponding flux uncertainties. We also determined a mean quality vector for each source, again using the flux uncertainty to construct weights. The formal uncertainty in each combined spectrum was determined by normal propagation of errors. Errors larger than the formal uncertainty may persist in the co-added spectra, especially near 3050 Å, where data quality flags do not always completely exclude data affected by reseau marks in the *IUE* cameras.

TABLE 1
PRE-MAIN-SEQUENCE STARS OBSERVED BY IUE WITH LW CAMERAS

ID3 ^a (1)	ID1 ^b (2)	HBC ^c (3)	Name ^d (4)	Alt. Name ^d (5)	Spectral Type ^e (6)	Category ^f (7)	N ^g (8)
1.....	(1)	329	VX Cas		A0,3eV	HAEBE	1
2.....	2	330	V594 Cas	MWC 419	B:eq	HAEBE	4
3.....	3	10	WY Ari	LkH α 264	K5 V(Li)	CTTS	3
4.....	HD 19745	CD -65 150	K1 III	nonPMS	1
(5).....	4	345	HH 12/107	SSS 107	M0:	CTTS	0
6.....	(5)	350	XY Per	HD 275877	Aep+sh	HAEBE	1
7.....	(7)	367	V773 Tau	HD 283447	K3 V(Li)	NTTS	4
8.....	...	23	FM Tau	Haro 6-1	M0	CTTS	1
9.....	...	25	CW Tau	MH α 259-3	K3 V(Li)	CTTS	4
10.....	8	29	V410 Tau	BD +28 637	K3 V(Li)	NTTS	10
11.....	...	376	V1069 Tau	NTTS 041559+1716	K7(Li)	NTTS	1
12.....	9	32	BP Tau	MH α 259-7	K7 V(Li)	CTTS	59
13.....	...	378	V819 Tau	WK1	K7 V(Li)	NTTS	1
14.....	10	33	DE Tau	MH α 259-8	M2: V(Li)	CTTS	8
15.....	11	34	RY Tau	BD +28 645	K1 IV,V(Li)	CTTS	83
16.....	12	380	V987 Tau	HD 283572	G5 IV(Li)	NTTS	9
17.....	13	35	T Tau	BD +19 706	K0 IV,V(Li)	CTTS	30
18.....	14	36	DF Tau	MH α 259-11	M0,1V(Li)	CTTS	22
19.....	15	37	DG Tau	MH α 259-10	M?	CTTS	18
20.....	(16)	388	V1072 Tau		K1(Li)	NTTS	2
21.....	...	39	DI Tau	MH α 259-9	M0 V(Li)	NTTS	1
22.....	17	43	UX Tau	BD +17 736	K2 V(Li)	CTTS	4
23.....	18	45	DK Tau	MH α 259-12	K7 V(Li)	CTTS	4
24.....	...	392	V1074 Tau	NTTS 042835+1700	K5(Li?)	NTTS	1
(25).....	(20)	49	HL Tau	Haro 6-14	K7,M2?	CTTS	0
26.....	...	397	V1075 Tau	NTTS 042916+1751	K7(Li)	NTTS	1
27.....	...	399	V827 Tau	FK2	K7,M0(Li)	NTTS	2
(28).....	...	400	V826 Tau	FK1	K7,M0(Li)	NTTS	0
29.....	...	54	GG Tau	MH α 257-2	K7 V(Li)	CTTS	6
30.....	V1147 Tau	HD 286839	K0	nonPMS	1
31.....	...	52	UZ Tau		M1,3: V(Li)	CTTS	1
(32).....	...	55	GH Tau	Haro 6-20	M2,3V(Li)	CTTS	0
33.....	...	404	V807 Tau	Elias 12	K7 V(Li)	CTTS	2
34.....	(21)	405	V830 Tau	WK2	K7,M0 V(Li)	NTTS	3
35.....	22	56	GI Tau	Haro 6-21	K6 V(Li)	CTTS	1
36.....	(23)	57	GK Tau	Haro 6-22	K7 V(Li)	CTTS	2
37.....	24	58	DL Tau	MH α 259-13	K7 V(Li)	CTTS	6
(38).....	...	60	HN Tau	Haro 6-24	K5	CTTS	0
39.....	...	408	V1110 Tau	Wa Tau/1	K0 IV	nonPMS	1
40.....	25	63	AA Tau	MH α 259-17	K7 V(Li)	CTTS	6
41.....	...	65	DN Tau	MH α 259-18	M0 V(Li)	CTTS	17
42.....	93 Tau	HD 29589	B8 IV	HAEBE	4
43.....	(26)	...	HD 283817	BD +24 676	A3e/G0e	HAEBE	1
44.....	...	72	DQ Tau	MH α 257-7	M0,1V(Li)	CTTS	1
45.....	...	73	V1001 Tau	Haro 6-37	K6	CTTS	1
46.....	27	74	DR Tau	MH α 257-8		CTTS	40
47.....	28	75	DS Tau	MH α 259-2	K5 V(Li)	CTTS	4
48.....	...	76	UY Aur		K7 V(Li)	CTTS	3
49.....	29	77	GM Aur	MH α 259-1	K3 V(Li)	CTTS	5
50.....	30	426	V396 Aur	LkCa 19	K0 V(Li)	NTTS	2
51.....	31	78	AB Aur	HD 31293	B9,A0e+sh	HAEBE	11
52.....	32	79	SU Aur	HD 282624	G2 III(Li)	CTTS	28
53.....	33	...	HD 31648	MWC 480	A2/3ep+sh	HAEBE	4
54.....	34	430	UX Ori	BD -4 1029	A3e III	HAEBE	13
55.....	...	82	LkH α 333		K5	CTTS	1
56.....	35	80	RW Aur	BD +30 792	K1:	CTTS	29
57.....	AE Aur	HD 34078	O9.5 Ve	HAEBE	5
58.....	36	...	V346 Ori	HD 287841	A5 III:e	HAEBE	1
59.....	...	84	CO Ori	Haro 6-44	F8:e V(Li)	CTTS	2
60.....	37	...	HD 35929	BD -8 1128	A5e	HAEBE	3
61.....	38	85	GW Ori	BD +11 819	G5(Li)	CTTS	10
62.....	...	86	V649 Ori	MH α 265-3	G8 III,V(Li)	CTTS	1
63.....	(39)	...	HD 36112	MWC 758	A3e	HAEBE	1
64.....	...	435	AB Dor	HD 36705	K0,2(Li)	NTTS	11

TABLE 1—Continued

ID3 ^a (1)	ID1 ^b (2)	HBC ^c (3)	Name ^d (4)	Alt. Name ^d (5)	Spectral Type ^e (6)	Category ^f (7)	N ^g (8)
65.....	40	94	HK Ori	MWC 497	B8/A4ep	HAEBE	2
66.....	(41)	436	RY Ori		F8:pe(Li)	CTTS	1
67.....	42	443	HD 245059	λ Ori X-1	K3 V:(Li)	NTTS	1
68.....	(43)	113	V1044 Ori	Parenago 1404	G5 IV,V(Li)	CTTS	1
69.....	...	114	EZ Ori	Parenago 1409	G0:n(Li)	CTTS	1
(70).....	Parenago 1539		A0	HAEBE	0
71.....	44	...	V372 Ori	HD 36917	A0 V	HAEBE	2
72.....	45	451	HD 245185	BD +9 880	A5e α	HAEBE	5
73.....	BD -5 1306		A2 Vp	HAEBE	1
74.....	HD 36939	Parenago 232	B9	HAEBE	2
(75).....	(46)	122	KM Ori	Parenago 1659	K1(Li)	NTTS	0
76.....	KS Ori		A0	HAEBE	1
(77).....	...	125	KR Ori	Parenago 1684	K6(Li)	CTTS	0
(78).....	47	126	LL Ori	Parenago 1746	K2,3(Li)	CTTS	0
79.....	HD 36981	Parenago 237	B5 V	HAEBE	3
80.....	49	...	LP Ori	HD 36982	B1.5 V	HAEBE	3
81.....	...	132	Parenago 1817		K2(Li)	NTTS	1
82.....	V1016 Ori	HD 37020	O7	HAEBE	3
(83).....	...	455	Parenago 1869		G5:(Li)	CTTS	0
84.....	BM Ori	HD 37021	B0 V	HAEBE	44
85.....	HD 37022		O6pe	HAEBE	7
86.....	...	456	MR Ori	Parenago 1885	A2 V	HAEBE	3
87.....	LZ Ori	HD 294263	A0	HAEBE	1
88.....	HD 37023		B0.5 Vp	HAEBE	3
(89).....	50	458	MT Ori	Parenago 1910	K3,4(Li)	NTTS	0
90.....	51	...	V1230 Ori	BD -5 1318	B8 IV-V	HAEBE	2
91.....	52	464	CQ Tau	HD 36910	A8ve α	HAEBE	7
92.....	43 Ori	HD 37041	O9.5 Vpe	HAEBE	10
93.....	HD 37042	ZI 435	B1 V	HAEBE	2
(94).....	(53)	...	NT Ori	Haro 4-241	K8e	CTTS	0
95.....	54	...	NU Ori	HD 37061	B1 V	HAEBE	5
96.....	(56)	471	NV Ori	BD -05 1324	F4,8III,V	NTTS	2
97.....	...	144	V360 Ori	Haro 4-84	K6	CTTS	1
98.....	V359 Ori	HD 37058	B3 Vp	HAEBE	2
99.....	59	154	T Ori	Haro 4-123	A3e α	HAEBE	4
100.....	HD 37114	NSV 2386	B8 V	HAEBE	1
101.....	60	482	BN Ori	HD 245465	F2,3e α	HAEBE	4
102.....	(62)	...	PR Ori	Haro 4-213	K4e	NTTS	1
103.....	63	164	V380 Ori	BD -06 1253	A1:e	HAEBE	12
104.....	64	167	BD -04 1191	Parenago 2441	G5:(Li)	CTTS	1
105.....	...	487	BD -06 1258	Parenago 2494	K0 IV(Li)	NTTS	1
106.....	65	169	BF Ori	Haro 4-229	A5e+sh	HAEBE	6
107.....	HD 37357	BD -6 1264	A0 Ve	HAEBE	1
108.....	66	170	RR Tau	AS 103	B8,9e α	HAEBE	3
109.....	67	...	HD 37490	ω Ori	B3 III/IVe	HAEBE	11
110.....	(68)	493	V350 Ori		A0e	HAEBE	2
111.....	69	...	HD 37806	MWC 120	B9 Ve+sh	HAEBE	8
112.....	...	181	DL Ori	Haro 7-3	K1	CTTS	1
113.....	70	...	V351 Ori	HD 38238	A7 III	HAEBE	2
114.....	71	186	FU Ori		G; I,II	FUOri	13
115.....	...	515	HD 288313	BD +1 1156	K2:n(Li)	NTTS	1
116.....	72	192	HD 250550	MWC 789	B9eq	HAEBE	16
117.....	73	193	LkH α 208		F0 Ve	HAEBE	1
118.....	74	...	FS CMa	HD 45677	B3[e]p+sh	HAEBE	22
119.....	75	202	VY Mon		B8:e	HAEBE	1
120.....	76	528	V699 Mon	LkH α 215	B7 IIne	HAEBE	1
121.....	77	529	HD 259431		B5:e	HAEBE	6
122.....	78	207	R Mon	BD +8 1427	B0e	HAEBE	2
(123).....	(79)	216	NX Mon	LH α 22	cont	CTTS	0
124.....	...	217	W84	VSB 59	F8,G0e	NTTS	1
125.....	80	219	V590 Mon	LH α 25	B8pe+sh	HAEBE	9
126.....	...	222	W108	VSB 78	F9:e(Li)	CTTS	1
(127).....	...	229	LX Mon	LH α 51	K7	CTTS	0
(128).....	...	238	MO Mon	LH α 72	K2	CTTS	0
129.....	81	...	HD 50138	MWC 158	B6 V[e]+sh	HAEBE	18

TABLE 1—Continued

ID3 ^a (1)	ID1 ^b (2)	HBC ^c (3)	Name ^d (4)	Alt. Name ^d (5)	Spectral Type ^e (6)	Category ^f (7)	N ^g (8)
130.....	82	...	OY Gem	HD 51585	B[e]	HAEBE	3
131.....	83	...	GU CMa	HD 52721	B2 Vne	HAEBE	2
132.....	84	243	Z CMa	HD 53179	B5/8neq+sh	HAEBE	6
133.....	85	...	HD 53367	MWC 166	B0 III/IVe	HAEBE	4
134.....	86	...	EW CMa	HD 56014	B3 IIIep	HAEBE	2
135.....	87	552	NX Pup	CoD –44 3318	F1:e	HAEBE	5
(136).....	HD 85567	He 3-331	B5 Vne	HAEBE	0
137.....	89	...	HD 87643	He 3-365	B3/4[e]	HAEBE	8
138.....	CPD –59 2854	WRA 15-689	B2/3Ve	HAEBE	2
139.....	91	...	GG Car	HD 94878	B5/6[e]+K3:	HAEBE	7
140.....	...	565	SY Cha	Sz 3	M0:	CTTS	2
141.....	...	567	TW Cha	Sz 5	M0:	CTTS	1
142.....	(92)	244	CR Cha	Sz 6	K2(Li)	CTTS	3
143.....	93	568	TW Hya	He 3-549	K7 V(Li)	CTTS	8
144.....	94	...	HD 95881	He 3-554	A1/2III/IVe	HAEBE	1
145.....	95	569	CS Cha	Sz 9	K5:	CTTS	2
146.....	...	570	CT Cha	Sz 11	K7:	CTTS	1
147.....	96	...	HD 96675	CHXR 16	B6 IV/V	HAEBE	1
148.....	(97)	245	DI Cha	Sz 19	G2 V(Li)	CTTS	2
149.....	98	575	VW Cha	Sz 24	K2	CTTS	3
150.....	99	246	CU Cha	HD 97048	A0pe+sh	HAEBE	7
151.....	(100)	578	VZ Cha	Sz 31	K6	CTTS	1
152.....	102	588	Sz 41	HJM E1-9a	K0	CTTS	1
153.....	103	247	CV Cha	LH α 332-21	G8 V(Li)	CTTS	5
154.....	104	...	HD 98922	He 3-644	B9 Ve	HAEBE	3
155.....	105	...	HD 100546	He 3-672	B9 Vne	HAEBE	3
156.....	HD 101412	He 3-692	B9.5 Ve	HAEBE	1
157.....	106	...	HD 104237	He 3-741	A4e	HAEBE	5
158.....	(107)	...	He 3-847	CPD –48 5215	B5e	HAEBE	1
(159).....	GSC 07798-00578			CTTS	0
160.....	108	...	He 3-1013	CPD –64 2939	Be	HAEBE	1
161.....	HD 130437	He 3-1031	B8 Ve	HAEBE	2
162.....	109	...	HD 132947	CPD –62 4379	A0e	HAEBE	1
163.....	...	597	IK Lup	Sz 65	K7,M0(Li)	CTTS	2
164.....	(110)	248	HT Lup	CoD –33 10685	K2 V(Li)	CTTS	4
165.....	...	249	GW Lup	Sz 71	M1.5	CTTS	1
166.....	(111)	...	HD 141569	BD –3 3833	A0 Ve	HAEBE	1
167.....	...	603	Sz 77		M0(Li)	CTTS	2
168.....	112	...	HD 142361	ScoPMS 5	G2 IV	NTTS	1
169.....	...	605	IM Lup	Sz 82	M0(Li)	CTTS	2
170.....	113	251	RU Lup	Sz 83	K	CTTS	23
171.....	114	...	HD 142666	BD –21 4228	A7/8Ve	HAEBE	2
172.....	...	606	Sz 126		K,M	CTTS	1
173.....	(115)	608	HD 143006	He 3-1126	G5	CTTS	1
174.....	...	609	He 3-1125	Sz 129	K7,M0	CTTS	1
175.....	116	252	RY Lup		K0,1V(Li)	CTTS	2
176.....	V1152 Sco	ScoPMS 21	K1 IV	NTTS	1
177.....	(117)	...	V1154 Sco	ScoPMS 23	K5 IV	NTTS	1
178.....	118	253	EX Lup		M0: V(Li)	CTTS	1
(179).....	(119)	...	V1156 Sco	ScoPMS 27	K2 IV	NTTS	0
180.....	120	612	HO Lup	Sz 88	M1	CTTS	1
181.....	121	...	HD 144432	He 3-1141	A7 Ve/F0e	HAEBE	2
182.....	...	615	Sz 96		M1.5	CTTS	1
183.....	122	616	HK Lup	Sz 98	K7,M0(Li)	CTTS	3
184.....	124	619	V856 Sco	HD 144668	A7e III, IV	HAEBE	18
(185).....	...	620	Sz 108	Eggen 2	M0.5	NTTS	0
(186).....	...	622	Sz 111	TH α 15-33	M0.5	CTTS	0
(187).....	...	631	Sz 124	TH α 15-43	M0	NTTS	0
188.....	125	254	V866 Sco A	AS 205	K5 V(Li)	CTTS	1
189.....	...	633	V1001 Sco	Wa Oph/2	K1 IV(Li)	NTTS	1
190.....	126	634	V1002 Sco	ScoPMS 52	K0 IV(Li)	NTTS	2
191.....	127	...	HD 146516	ScoPMS 60	G0 IV	NTTS	2
192.....	...	256	V895 Sco	Haro 1-1	K5,7	CTTS	1
(193).....	...	636	V2245 Oph	ROX 3	M0	NTTS	0
194.....	...	259	V2058 Oph	AS 206	K6,7	CTTS	1

TABLE 1—Continued

ID3 ^a (1)	ID1 ^b (2)	HBC ^c (3)	Name ^d (4)	Alt. Name ^d (5)	Spectral Type ^e (6)	Category ^f (7)	N ^g (8)
(195).....	...	637	Haro 1-6	DoAr 21	G,K	NTTS	0
196.....	128	...	He 3-1191	WRA 15-1484	B0:[e]	HAEBE	1
(197).....	...	641	ROX 20-2 se		M	NTTS	0
(198).....	...	263	V2247 Oph	SR 12	M1,2	NTTS	0
199.....	129	264	V2129 Oph	AS 207	K5,7	CTTS	2
200.....	...	265	V2059 Oph	SR 10	M1.5	CTTS	1
201.....	...	266	V853 Oph	SR 13	M1.5	CTTS	2
202.....	...	268	Haro 1-16	DoAr 44	K2,3	CTTS	1
(203).....	(130)	646	V346 Nor	HH57/IRS 8	F8eq III(Li)	FUOri	0
204.....	...	647	V2248 Oph	DoAr 51	M0:	NTTS	1
205.....	(131)	...	HD 150193	MWC 863	A0/4Ve	HAEBE	1
206.....	132	270	V1121 Oph	He 3-1260	K5(Li)	CTTS	2
207.....	133	271	AK Sco	HD 319139	F5 Ve(Li)	CTTS	7
208.....	134	655	V921 Sco	CoD -42 11721	B0[e]p	HAEBE	1
209.....	135	...	HD 326823	He 3-1330	B1.5[e]	HAEBE	1
210.....	136	273	KK Oph	TH α 27-3	A5 Ve	HAEBE	3
211.....	(137)	...	HD 327083	He 3-1359	B1.5e	HAEBE	3
212.....	138	...	He 3-1357	CPD -59 6926	B0/3e	nonPMS	8
213.....	139	...	He 3-1428	CD -49 11554	B0e	HAEBE	2
214.....	141	...	HD 316285	He 3-1482	B2/3[e]+sh	HAEBE	2
215.....	142	...	HD 163296	He 3-1524	A0/2Vep+sh	HAEBE	10
216.....	143	662	V4046 Sgr	HD 319139	K5,6Vn(Li)	CTTS	6
217.....	144	663	FK Ser	BD -10 4662	K5p V(Li)	CTTS	2
218.....	145	282	VV Ser	IrCh 21	B,Ae	HAEBE	2
219.....	146	286	S CrA		K6:	CTTS	1
220.....	...	676	V709 CrA	Wa CrA/1	K0,2 IV(Li)	NTTS	1
221.....	147	287	TY CrA	CoD -37 13024	B9	HAEBE	3
222.....	148	288	R CrA		A5:e+sh	HAEBE	3
(223).....	149	678	V702 CrA	Wa CrA/2	G8 IV:(Li)	NTTS	0
224.....	150	...	HD 179218	MWC 614	B9/A0 IV/Ve	HAEBE	1
225.....	152	686	WW Vul	BD +20 4136	A0,3Ve	HAEBE	7
226.....	153	...	V1295 Aql	HD 190073	A0 IVep+sh	HAEBE	8
227.....	154	689	V1685 Cyg	MWC 340	B2,3e+sh	HAEBE	1
(228).....	155	297	V751 Cyg	LkH α 170	A5:e	HAEBE	0
(229).....	...	300	V1057 Cyg	LkH α 190	A-Ge	FUOri	0
230.....	...	302	V1331 Cyg	LkH α 120	cont	CTTS	3
231.....	156	726	HD 200775	MWC 361	B3eq	HAEBE	3
232.....	157	730	BD +65 1637		B2,3nne	HAEBE	1
233.....	158	309	V373 Cep	LkH α 234	B5,7e	HAEBE	2
234.....	159	310	V1578 Cyg	BD +46 3471	A4:e+sh	HAEBE	1
(235).....	...	313	V375 Lac	LkH α 233	A7e α	HAEBE	0
236.....	160	315	DI Cep	MH α 47-30	G8 V:(Li)	CTTS	2
237.....	(161)	317	MWC 1080		B0?eq	HAEBE	1
238.....	BP Psc	IRAS 23198-0230		CTTS ^h	1

^a Internal identification number, enclosed in parentheses if none of the LW spectra are useful.^b Identification number from Paper I, enclosed in parentheses if none of the SW spectra were useful.^c Catalog number from Herbig & Bell 1988.^d Names in cols. (4) and (5) were selected from Paper I or using the catalog precedence specified therein.^e Spectral types preferentially from Herbig & Bell 1988 for TTS and Thé et al. 1994 for HAEBE stars.^f PMS category.^g Number of useful *IUE* LW spectra.^h We analyze as a CTTS, despite a HAEBE classification by Gregorio-Hetem et al. 1992.

2.3. Spectral Atlas

Figure 1 presents co-added LW spectra for 107 TTS with useful *IUE* data. Stars are ordered by right ascension, as in Table 1. Each panel is labeled with an identification number and name from Table 1. The typeface for each label reflects whether the star was categorized as CTTS/FUOri (*roman type*) or NTTS (*italic type*) in Table 1. Sources with no useful spectra (indicated by a zero in the last column of Table 1) do not appear in Figure 1. All spectra are presented on a

common wavelength scale, given at the bottom of each column. A flux scale factor of 10^{-14} erg s $^{-1}$ cm $^{-2}$ Å $^{-1}$ applies to all TTS spectra, though the flux range for each panel is given separately. Many TTS spectra are dominated by the unresolved Mg II doublet at 2800 Å. In order to highlight weaker spectral features, we ignored the wavelength interval containing Mg II when selecting the plot ranges in Figure 1. For noisy spectra, a horizontal dashed line indicates the zero flux level, so that the scatter below this level can be used to visually estimate noise levels. A few spectra are dominated

TABLE 2
ADDITIONAL CLASSIFICATIONS FROM THE LITERATURE

ID ^a (1)	Name (2)	Category (3)	Reason (4)	Reference (5)
4.....	HD 19745	nonPMS	Lithium-rich giant	1
7.....	V773 Tau	NTTS	No significant NIR or <i>B</i> -band excess	2
16.....	V987 Tau	NTTS	No IR excess or accretion signatures	3
22.....	UX Tau	CTTS	UX Tau A CTTS, B & C NTTS	4
30.....	V1147 Tau	nonPMS	No lithium absorption	5
39.....	V1110 Tau	nonPMS	No lithium absorption	6
75.....	KM Ori	NTTS	No NIR excess	7
83.....	Parenago 1869	CTTS	Orion PROPLYD	8
89.....	MT Ori	NTTS ^b	No NIR excess	7
94.....	NT Ori	CTTS	75 Å H α EW	9
105.....	BD -06 1258	NTTS	No NIR excess	10
124.....	W84	NTTS	Mg II absorption	11
126.....	W108	CTTS	Broad (>500 km s $^{-1}$) H α emission	12
163.....	IK Lup	CTTS	19 Å H α EW	13
169.....	IM Lup	CTTS	Red shifted absorption in H α	14
172.....	Sz 126	CTTS	Balmer series in emission (35 Å H γ EW)	13
176.....	V1152 Sco	NTTS	No NIR Excess	15
189.....	V1001 Sco	NTTS	No accretion signatures	16
190.....	V1002 Sco	NTTS	No accretion signatures	16
212.....	He 3-1357	nonPMS	Planetary nebula	17
220.....	V709 CrA	NTTS	No accretion signatures	16
223.....	V702 CrA	NTTS	No accretion signatures	16

^a Identification number from first column of Table 1.

^b Status is uncertain as Hillenbrand et al. 1998 detect weak emission in the Ca II 8542 Å line, possibly indicating accretion.

REFERENCES.—(1) Gregorio-Hetem et al. 1992; (2) Ghez et al. 1997; (3) Walter et al. 1987; (4) White & Ghez 2001; (5) Li & Hu 1998; (6) Martin et al. 1994; (7) Stassun et al. 2001; (8) O'Dell & Wen 1994; (9) Pravdo & Angelini 1993; (10) Rydgren & Vrba 1984; (11) this paper; (12) Fernandez & Miranda 1998; (13) Appenzeller et al. 1983; (14) Reipurth et al. 1996; (15) Walter et al. 1994; (16) Walter 1986; (17) Feibelman 1995.

by noise, but all have at least one real spectral feature (e.g., DI Tau, no. 21) or significant continuum (e.g., W84, no. 124).

Figure 2 presents co-added LW spectra for 97 HAEBE stars with useful *IUE* data. Note that the flux scale factor (10^{-13} erg s $^{-1}$ cm $^{-2}$ Å $^{-1}$) is 10 times larger than in Figure 1. Spectra are ordered by spectral type (see § 3.4) to emphasize the striking differences between stars of similar spectral type, for example HK Ori (A1, no. 65), HD 163296 (A1, no. 215), and VX Cas (A1.5, no. 1). Continuum is clearly detected in all HAEBE stars. Spectral lines are rare in the hottest stars, becoming more common with decreasing temperature. Spectral lines can appear in emission or absorption. A broad graphite extinction feature near 2200 Å is present in many spectra of HAEBE stars, for example AE Aur (O9.5, no. 57). Some stars have a rise in flux shortward of 2400 Å that may be due in part to a calibration error, rather than extinction. Because sensitivity drops quickly at the shortest wavelengths, a small error in background subtraction can leave a residual count rate that would mimic a flux spectrum rising toward the shortest wavelengths. Appropriate caution is advised.

Our co-added *IUE* spectra of TTS and HAEBE stars are available electronically² from the Multi-Mission Archive

at Space Telescope (MAST). Co-added main-sequence templates described in § 3.3 are also available at the same site.

2.4. Flux Variability

A detailed analysis of potentially interesting temporal variations is beyond the scope of this atlas, but as in Paper I, we report the amplitude and statistical significance of flux variations in 127 stars with more than one useful *IUE* spectra. We applied the methodology described in § 2.3 of Paper I to fluxes integrated over the wavelength interval 1900–3200 Å. Refer to Paper I for details of the analysis and an explanation of the measured quantities, except that Paper I should have stated that the hypothesis of null variation implies $\alpha = 0$, not $\alpha = 1$, where α is a measure of the fractional change in the flux of a single exposure relative to the mean for all exposures. The results in Paper I are correct nonetheless.

Table 3 gives results of the variability analysis, ordered by decreasing significance of variability. The first four columns reiterate information from Table 1. Column (5) contains χ^2_{ν} for a model assuming no variability. Large χ^2_{ν} values imply a poor model fit or equivalently the presence of significant variations. The last two columns of Table 3 give the fractional variability amplitude (A) in percent and the associated uncertainty (σ_A). When the measured value of A is less than $2\sigma_A$, we present the result as a 2 σ upper limit on A . Since A is defined as variation relative to the mean, values of

² See <http://archive.stsci.edu/prepds/iuepms/>.

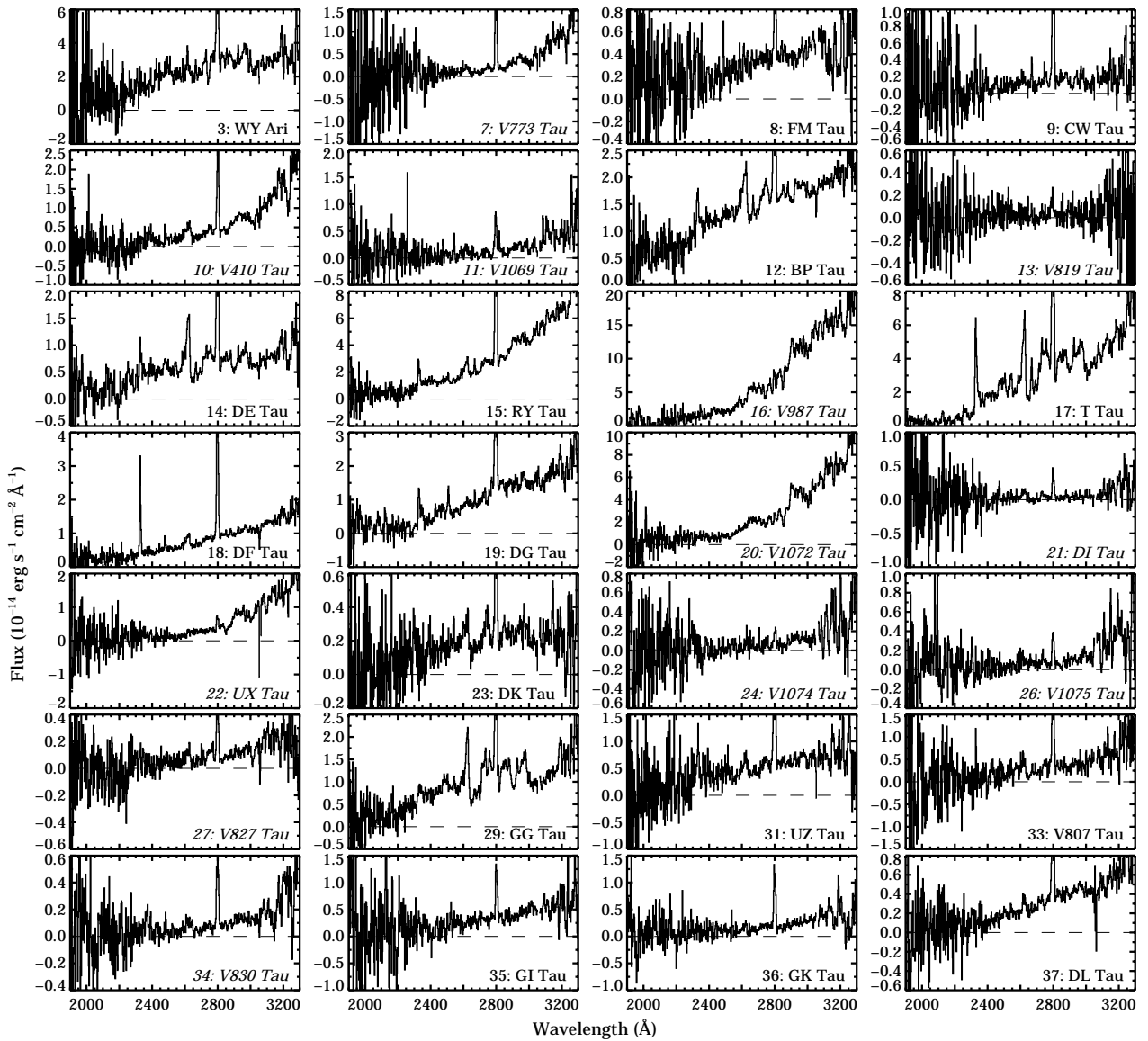


FIG. 1.—Combined LW spectra of every TTS with useful *IUE* data. Each source name is preceded by an identification number and is set in a typeface that distinguishes between CTTS (*roman type*) and NTTS (*italic type*). For noisy sources, the zero flux level is indicated by a horizontal dashed line. Histogram breaks occur where data quality flags indicate bad data.

A significantly larger than 100% are unlikely, even when brightness varies by factors of a few. We discuss these variability results in § 4.

3. ANALYSIS

3.1. NTTS Templates

NTTS are useful proxies for the intrinsic stellar component of CTTS. Removing a properly scaled and reddened NTTS template spectrum from a CTTS spectrum leaves only the excess associated with accretion and outflows. To construct NTTS templates, we first dereddened spectra of each NTTS observed by *IUE* with literature values of A_V listed in the last five columns of Table 4. When more than one value of A_V is listed for a particular star, we adopted the first value in the corresponding row. The identification number and spectral class of each NTTS are repeated from Table 1.

After interpolating the dereddened NTTS spectra onto a common wavelength scale, we normalized each spectrum by the total flux in the wavelength interval 2500–3200 \AA , excluding the Mg II region 2775–2825 \AA . We then compared each individual spectrum with the mean of all spectra, noting two slightly different groups of residuals. N1 templates resemble G type NTTS with weak Fe II absorption near 2600 \AA and gradually rising continuum at the longest wavelengths. N2 templates resemble K type NTTS with deeper Fe II absorption near 2600 \AA and a steeper rise beyond 3000 \AA . Template classifications are not a strict function of spectral class because spectral characteristics also depend on magnetic activity level. The third column of Table 4 lists the template type of each NTTS, unless excessive noise or an unusual continuum shape precludes classification.

Use of an individual NTTS spectrum to model a CTTS would introduce noise. Because NTTS spectra within the N1 and N2 groups are similar, we constructed a single

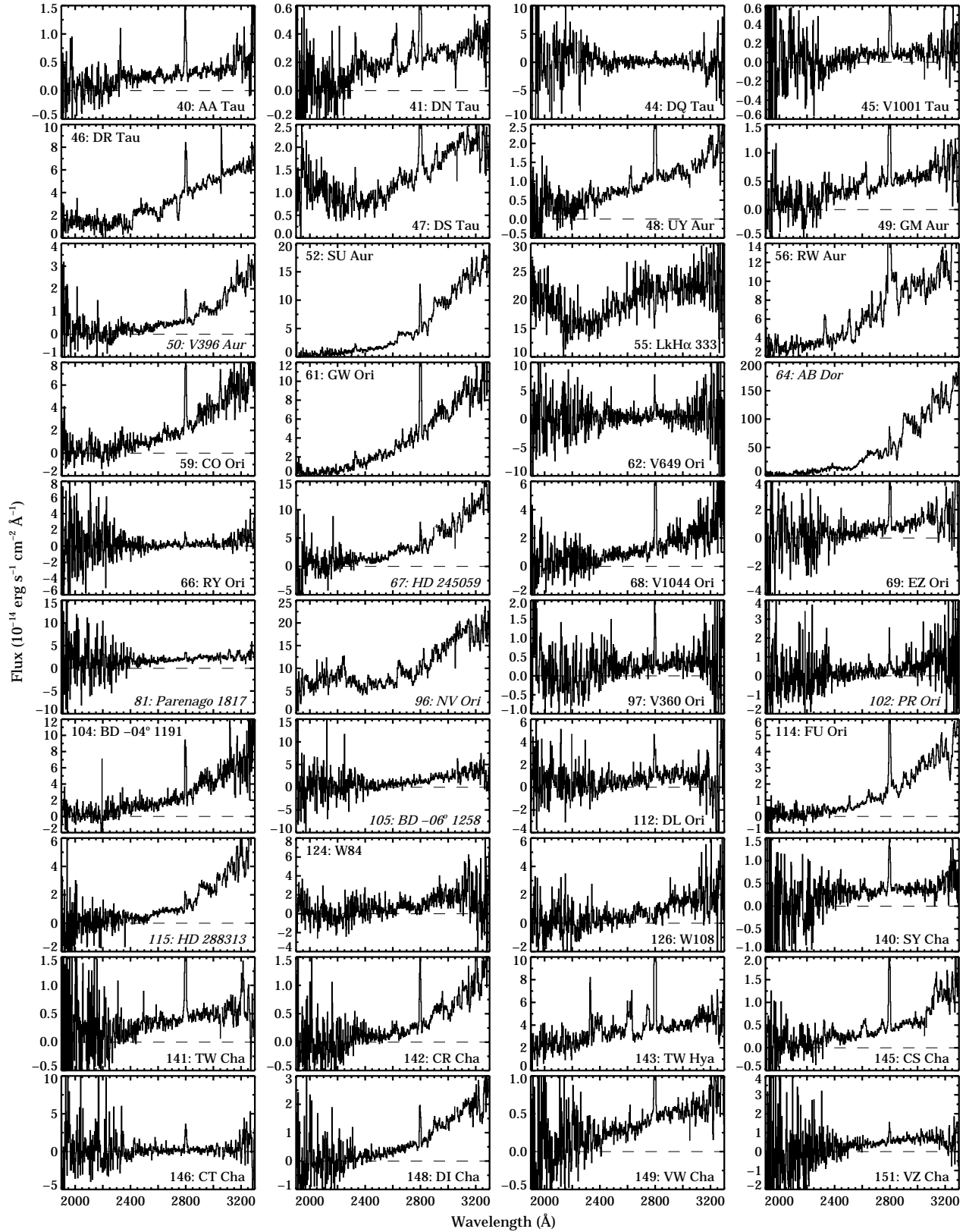


FIG. 1.—Continued

weighted-mean spectrum for each group. To remove outliers that would compromise least-squares fits, we applied a 5 pixel wide median filter to the mean template spectra. As shown in Figure 3, the resulting NTTS template spectra are distorted locally but are free of major noise excursions.

These N1 and N2 templates are used in the next section to model CTTS spectra. We also used the two NTTS templates to determine $A_V = 0.5 \pm 0.2$ for AB Dor (no. 64) and $A_V = 1.0 \pm 0.5$ for HD 288313 (no. 115), neither of which have A_V values in the references cited in Table 4.

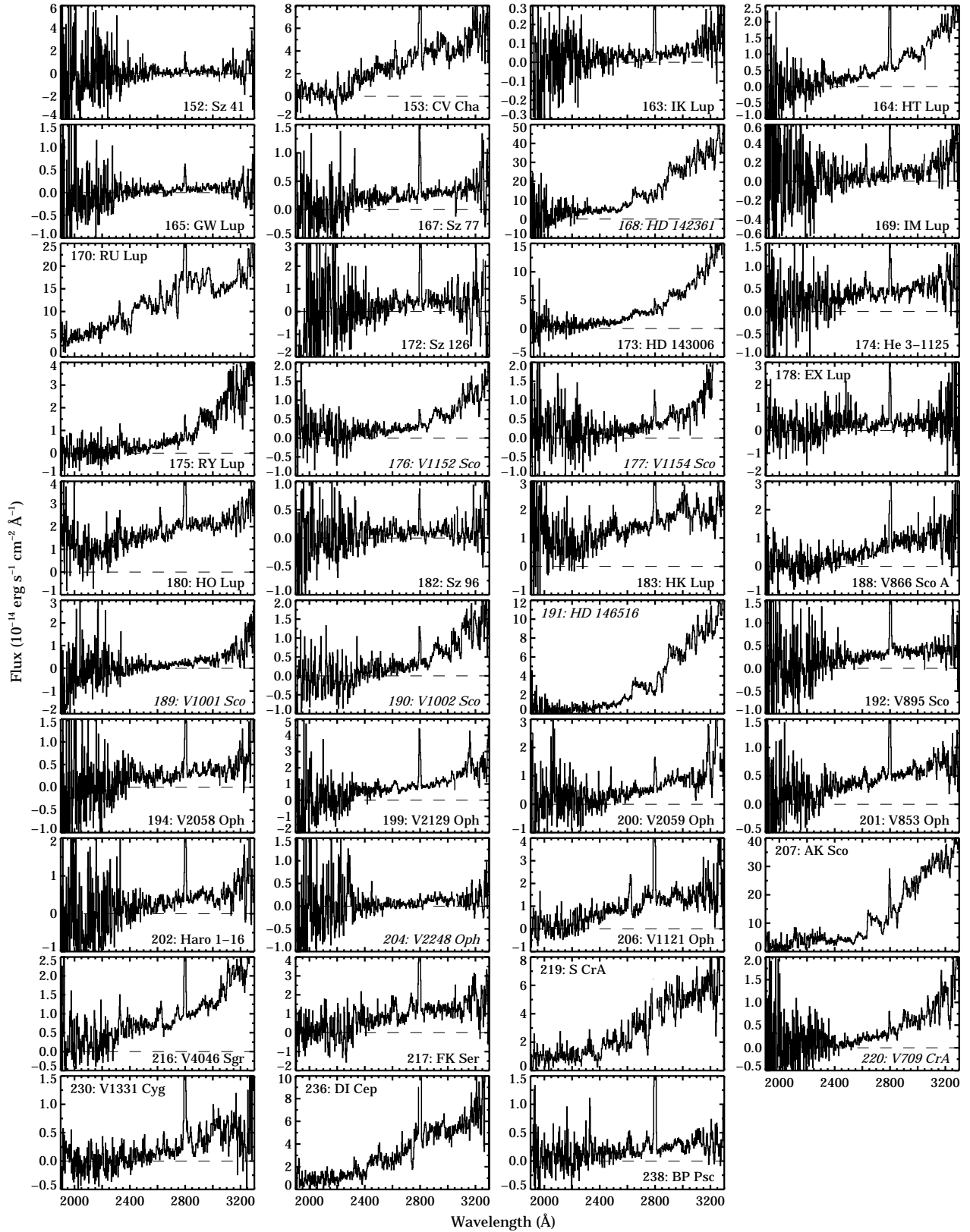


FIG. 1.—Continued

3.2. CTTS Continuum and Line Emission

In Paper II we argued that most SW emission from CTTS is due to accretion related processes. Here we measure LW emission fluxes, which may also trace accretion, despite a

larger contribution from the active photosphere. For each co-added CTTS spectrum, we calculated the mean continuum flux per \AA in two wavelength intervals relatively free of strong spectral lines. Table 6 presents logarithms of the mean flux in the wavelength intervals 2200–2315 \AA

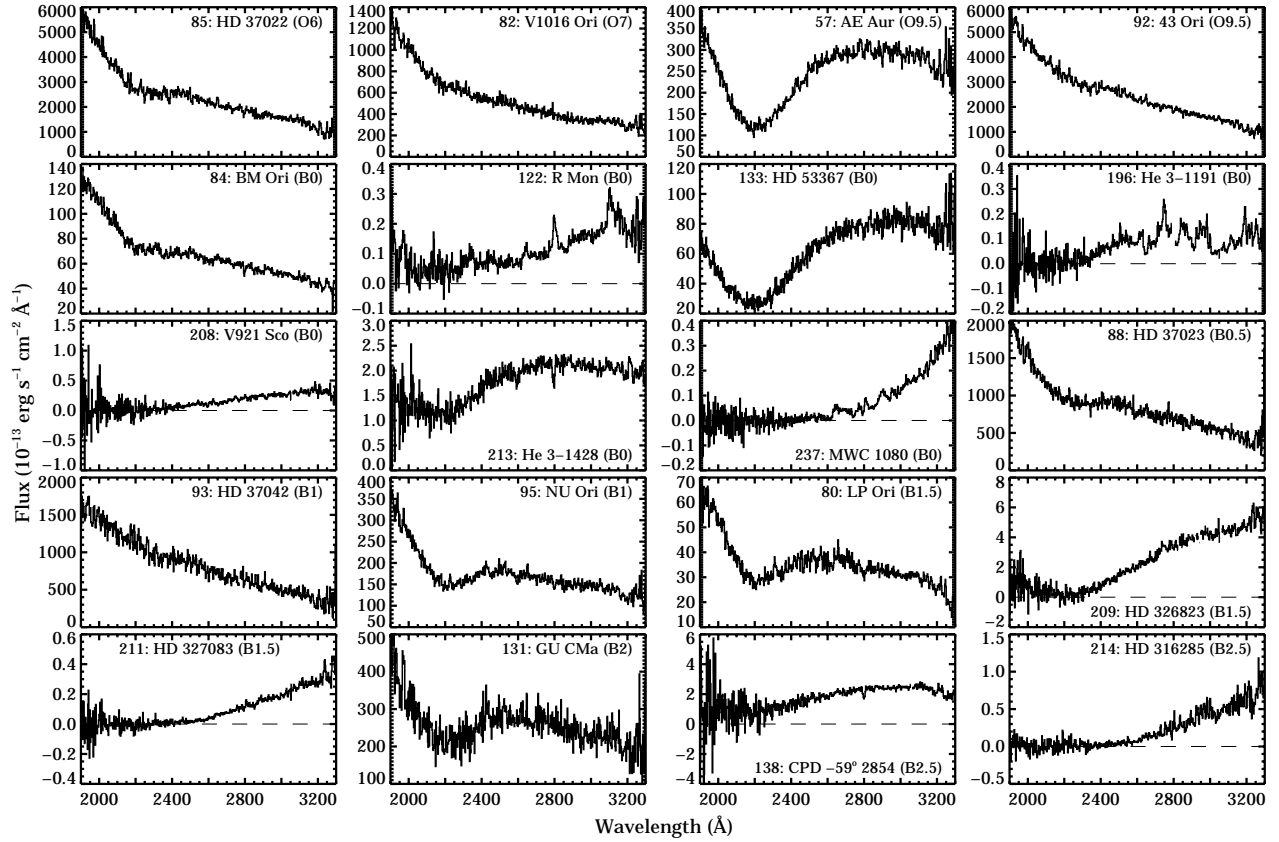


FIG. 2.—Combined LW spectra of every HAEBE star with useful *IUE* data. Each source name is preceded by an identification number. For noisy sources, the zero flux level is indicated by a horizontal dashed line. Histogram breaks occur where data quality flags indicate bad data.

(“cnt2257”) and 2995–3125 Å (“cnt3060”). Throughout the table, parentheses enclose the formal uncertainty in the two least significant digits, unless a 2σ upper limit is quoted. Figure 4 shows the extent and spectral content of these two pseudo-continuum windows for T Tau (no. 17).

Figure 4 also illustrates that LW spectra of CTTS may contain prominent emission lines. Because individual spectral lines generally are not resolved in *IUE* low-resolution spectra, we defined seven wavelength intervals bounded by pseudo-continuum and dominated by emission from one ionic species. These wavelength intervals and species are listed in Table 5 and indicated in Figure 4. To facilitate line identification and to demonstrate the quality of *IUE* data, Figure 4 also shows a STIS G230L spectrum (data set o5sex05020) of T Tau degraded to 6 Å resolution and multiplied by a polynomial to match the observed *IUE* continuum. Note that NEWSIPS and *HST* use different flux calibration standards (Massa & Fitzpatrick 2000), so the two need not agree.

In order to measure excess line emission due to accretion, the underlying active photospheric spectrum must be characterized. We therefore fitted CTTS spectra with the reddened sum of an NTTS template plus a schematic veiling continuum, considering wavelengths in the interval 2160–3165 Å, but excluding the spectral line windows in Table 5. Ideally a detailed physical model would be used to generate a family of realistic veiling continua, but excess line emission can be measured using any simple function that reproduces the observed pseudo-continua of CTTS. We used a quadratic polynomial to approximate crudely the continuum excess in CTTS.

Figure 5 shows a sample continuum fit for CS Cha (no. 63). Fitted models are often dominated by the NTTS template or the quadratic veiling continuum, but in CS Cha the two components are comparable. We do not tabulate model veiling or reddening values because LW *IUE* spectra alone are not always sufficient to separate these parameters. For example, the quadratic continuum excess is negative in some cases. Nonetheless, the sum of the two components fitted all CTTS spectra well. For each CTTS, we compared fits using NTTS templates N1 and N2, selecting the fit with significantly lower χ^2_r or averaging the two fits if χ^2_r differed by less than 5%. All model fits were inspected visually to ensure accuracy.

For each observed CTTS spectrum, we computed excess flux above the model pseudo-continuum, integrating across the emission line windows listed in Table 5. Figure 4 presents graphically the integration intervals, while Figure 5 highlights portions of the CTTS flux spectrum above the fitted pseudo-continuum. Emission line fluxes and associated uncertainties are given in $\text{ergs s}^{-1} \text{cm}^{-2}$ in the last seven columns of Table 6, which have header labels from column (4) of Table 5. Note the scale factor at the top of each column. We calculated uncertainties by propagating measurement errors for pixels used to compute the line flux. Labels at the top of each column indicate the dominant ionic species in each wavelength interval, but minority species may also contribute significantly. In particular, the C II] region also contains Fe II, and possibly a small contribution from C II (Wiese, Fuhr, & Deters 1996), but C II] is expected to dominate in all cases. Similar considerations apply to the other emission line windows.

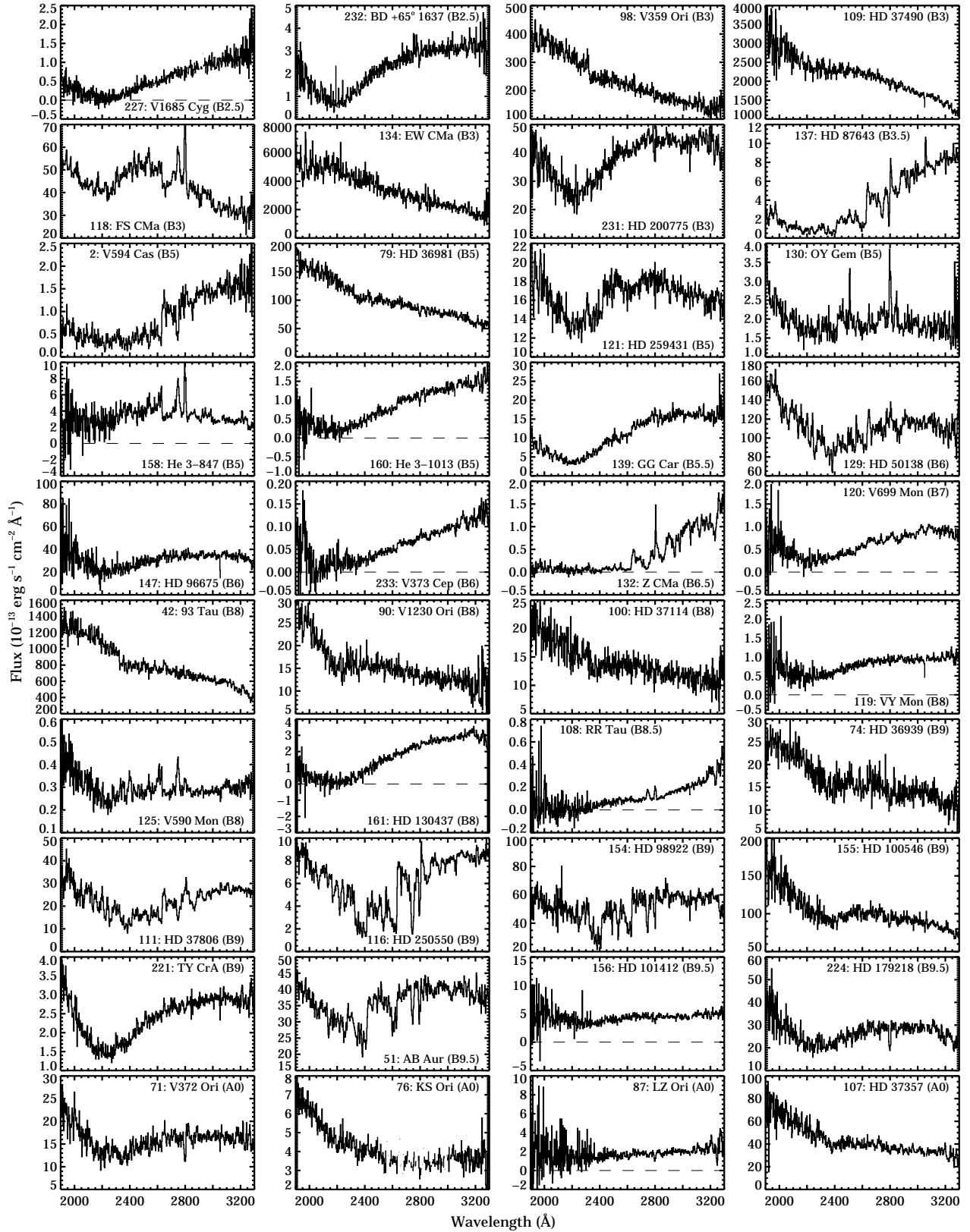


FIG. 2.—Continued

3.3. Main-Sequence Analogs of HAEBE Stars

Spectroscopic evidence of accretion onto HAEBE stars is rare at best. Outflow signatures are more common, but still not ubiquitous. To study spectral peculiarities associated with the youth of HAEBE stars, ordinary comparison stars of the same spectral class are useful. We therefore constructed a LW spectral library of normal main-sequence stars for spectral types O3 V to F5 V.

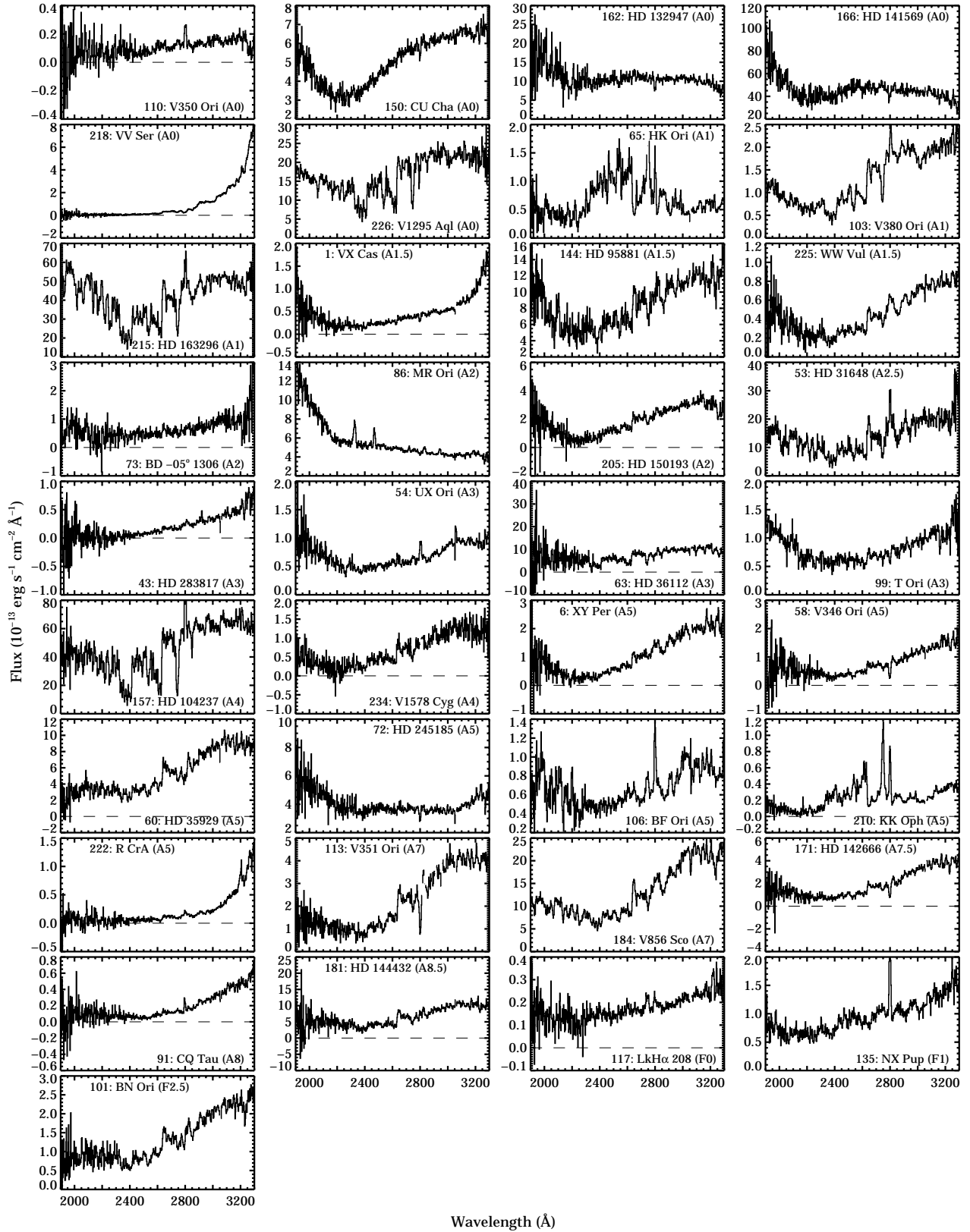


FIG. 2.—Continued

We generally adopted template stars from Table 9 of Paper I, but LW spectra were inadequate or unavailable for five SW templates stars. For these missing templates and for spectral classes outside the range covered in Paper I, we

searched the *IUE* merged log for new template stars. With no comprehensive catalog of coordinates to drive the search, we instead relied on object classes and spectral types in the *IUE* merged log. Specifically, we searched for *IUE*

TABLE 3
MEASURED FLUX VARIATIONS

ID ^a (1)	Name (2)	Category ^b (3)	N ^c (4)	χ^2_f (5)	A ^d (6)	σ_A (7)
88.....	HD 37023	HAEBE	3	10623.3	83.9	0.6
48.....	UY Aur	CTTS	3	358.9	67.0	2.5
106.....	BF Ori	HAEBE	6	274.3	52.7	1.4
171.....	HD 142666	HAEBE	2	259.6	45.4	2.8
170.....	RU Lup	CTTS	23	195.7	46.9	0.8
56.....	RW Aur	CTTS	29	176.2	53.6	0.8
183.....	HK Lup	CTTS	3	173.3	58.7	3.8
80.....	LP Ori	HAEBE	3	164.9	40.5	2.3
132.....	Z CMa	HAEBE	6	156.4	43.7	1.7
54.....	UX Ori	HAEBE	13	129.2	44.0	1.3
206.....	V1121 Oph	CTTS	2	122.8	36.7	3.3
225.....	WW Vul	HAEBE	7	112.3	34.0	1.7
84.....	BM Ori	HAEBE	44	112.2	36.9	0.6
122.....	R Mon	HAEBE	2	101.5	34.1	3.4
109.....	HD 37490	HAEBE	11	92.8	34.2	1.3
99.....	T Ori	HAEBE	4	82.0	33.8	2.2
59.....	CO Ori	CTTS	2	78.0	28.3	3.6
108.....	RR Tau	HAEBE	3	73.2	49.8	4.3
18.....	DF Tau	CTTS	22	55.9	40.9	1.4
96.....	NV Ori	NTTS	2	51.1	24.9	3.5
92.....	43 Ori	HAEBE	10	47.3	19.9	1.4
47.....	DS Tau	CTTS	4	42.6	30.1	3.2
16.....	V987 Tau	NTTS	9	41.8	28.4	1.9
86.....	MR Ori	HAEBE	3	40.9	19.8	2.9
15.....	RY Tau	CTTS	83	34.6	31.9	0.7
46.....	DR Tau	CTTS	40	34.4	29.2	1.1
82.....	V1016 Ori	HAEBE	3	28.0	19.2	2.7
184.....	V856 Sco	HAEBE	18	27.6	23.9	1.3
222.....	R CrA	HAEBE	3	27.3	23.2	3.5
91.....	CQ Tau	HAEBE	7	27.0	24.8	2.6
49.....	GM Aur	CTTS	5	23.4	26.9	4.0
12.....	BP Tau	CTTS	59	23.2	28.8	0.9
236.....	DI Cep	CTTS	2	20.7	16.1	3.6
149.....	VW Cha	CTTS	3	20.4	33.4	5.4
17.....	T Tau	CTTS	30	20.1	23.6	1.3
129.....	HD 50138	HAEBE	18	20.1	18.7	1.2
201.....	V853 Oph	CTTS	2	19.8	29.2	6.6
2.....	V594 Cas	HAEBE	4	19.6	19.1	2.6
40.....	AA Tau	CTTS	6	16.9	33.4	4.4
207.....	AK Sco	CTTS	7	15.6	18.1	2.1
22.....	UX Tau	CTTS	4	15.5	33.1	5.8
217.....	FK Ser	CTTS	2	15.4	28.1	7.4
135.....	NX Pup	HAEBE	5	14.1	13.9	2.2
167.....	Sz 77	CTTS	2	13.1	28.8	8.0
175.....	RY Lup	CTTS	2	12.8	16.3	4.6
140.....	SY Cha	CTTS	2	12.8	41.0	11.8
118.....	FS CMa	HAEBE	22	12.2	13.3	1.1
233.....	V373 Cep	HAEBE	2	11.9	13.7	4.0
153.....	CV Cha	CTTS	5	11.0	16.2	2.7
216.....	V4046 Sgr	CTTS	6	10.4	17.3	3.3
51.....	AB Aur	HAEBE	11	10.4	12.5	1.5
139.....	GG Car	HAEBE	7	10.3	12.7	2.1
19.....	DG Tau	CTTS	18	9.8	17.6	1.7
37.....	DL Tau	CTTS	6	9.7	29.6	6.2
23.....	DK Tau	CTTS	4	9.1	33.4	9.9
164.....	HT Lup	CTTS	4	8.3	22.1	4.7
221.....	TY CrA	HAEBE	3	8.2	11.4	2.9
52.....	SU Aur	CTTS	28	8.1	13.1	1.1
29.....	GG Tau	CTTS	6	8.0	22.0	3.9
137.....	HD 87643	HAEBE	8	7.6	11.9	2.0
143.....	TW Hya	CTTS	8	7.5	17.0	3.0
41.....	DN Tau	CTTS	17	7.1	25.5	3.1
14.....	DE Tau	CTTS	8	7.0	14.7	2.9
10.....	V410 Tau	NTTS	10	6.2	22.8	3.7
65.....	HK Ori	HAEBE	2	5.5	8.3	3.7
211.....	HD 327083	HAEBE	3	5.3	18.0	5.8
3.....	WY Ari	CTTS	3	5.0	13.2	4.2

TABLE 3—Continued

ID ^a (1)	Name (2)	Category ^b (3)	N ^c (4)	χ^2_f (5)	A ^d (6)	σ_A (7)
72.....	HD 245185	HAEBE	5	4.6	8.7	2.3
103.....	V380 Ori	HAEBE	12	4.6	8.5	1.5
116.....	HD 250550	HAEBE	16	4.4	8.1	1.3
74.....	HD 36939	HAEBE	2	3.9	<7.5	3.8
226.....	V1295 Aql	HAEBE	8	3.6	7.1	1.8
210.....	KK Oph	HAEBE	3	3.6	6.8	3.1
215.....	HD 163296	HAEBE	10	3.5	7.5	1.6
61.....	GW Ori	CTTS	10	3.4	7.4	1.7
199.....	V2129 Oph	CTTS	2	3.1	<15.0	7.5
64.....	AB Dor	NTTS	11	2.9	7.5	1.7
114.....	FU Ori	FUOri	13	2.8	7.6	1.8
190.....	V1002 Sco	NTTS	2	2.6	<16.3	8.2
230.....	V1331 Cyg	CTTS	3	2.6	<10.3	5.1
191.....	HD 146516	NTTS	2	2.5	<7.6	3.8
50.....	LkCa 19	NTTS	2	2.4	<16.5	8.3
110.....	V350 Ori	HAEBE	2	2.3	<12.3	6.2
163.....	IK Lup	CTTS	2	1.8	<72.4	36.2
218.....	VV Ser	HAEBE	2	1.7	<9.6	4.8
53.....	HD 31648	HAEBE	4	1.5	<5.1	2.5
34.....	V830 Tau	NTTS	3	1.5	<23.2	11.6
111.....	HD 37806	HAEBE	8	1.3	4.8	1.8
9.....	CW Tau	CTTS	4	1.2	<28.6	14.3
157.....	HD 104237	HAEBE	5	1.2	5.0	2.3
125.....	V590 Mon	HAEBE	9	1.1	4.9	1.8
154.....	HD 98922	HAEBE	3	0.9	<5.9	3.0
150.....	CU Cha	HAEBE	7	0.9	4.0	1.9
20.....	V1072 Tau	NTTS	2	0.9	<9.0	4.5
33.....	V807 Tau	CTTS	2	0.8	<40.0	20.0
148.....	DI Cha	CTTS	2	0.8	<13.3	6.7
57.....	AE Aur	HAEBE	5	0.8	<4.6	2.3
169.....	IM Lup	CTTS	2	0.7	<68.1	34.1
85.....	HD 37022	HAEBE	7	0.7	<3.8	1.9
142.....	CR Cha	CTTS	3	0.7	<15.9	7.9
93.....	HD 37042	HAEBE	2	0.6	<7.1	3.6
113.....	V351 Ori	HAEBE	2	0.5	<7.4	3.7
133.....	HD 53367	HAEBE	4	0.4	<5.0	2.5
121.....	HD 259431	HAEBE	6	0.4	<4.2	2.1
7.....	V773 Tau	NTTS	4	0.4	<25.2	12.6
60.....	HD 35929	HAEBE	3	0.4	<6.1	3.1
130.....	OY Gem	HAEBE	3	0.3	<5.9	2.9
27.....	V827 Tau	NTTS	2	0.3	<26.7	13.3
231.....	HD 200775	HAEBE	3	0.3	<5.9	2.9
101.....	BN Ori	HAEBE	4	0.3	<5.4	2.7
145.....	CS Cha	CTTS	2	0.3	<13.3	6.6
134.....	EW CMa	HAEBE	2	0.3	<7.1	3.6
181.....	HD 144432	HAEBE	2	0.2	<7.9	4.0
131.....	GU CMa	HAEBE	2	0.2	<7.2	3.6
95.....	NU Ori	HAEBE	5	0.2	<4.5	2.2
71.....	V372 Ori	HAEBE	2	0.1	<7.2	3.6
214.....	HD 316285	HAEBE	2	0.1	<8.4	4.2
79.....	HD 36981	HAEBE	3	0.1	<5.8	2.9
155.....	HD 100546	HAEBE	3	0.1	<5.9	3.0
138.....	CPD -59 2854	HAEBE	2	0.1	<8.3	4.1
42.....	93 Tau	HAEBE	4	0.1	<5.1	2.5
36.....	GK Tau	CTTS	2	0.0	<25.1	12.6
161.....	HD 130437	HAEBE	2	0.0	<7.6	3.8
90.....	V1230 Ori	HAEBE	2	0.0	<7.2	3.6
213.....	He 3-1428	HAEBE	2	0.0	<7.3	3.6
98.....	V359 Ori	HAEBE	2	0.0	<7.1	3.6

^a Identification number from first column of Table 1.

^b PMS category from seventh column of Table 1.

^c Number of good IUE spectra used in analysis.

^d Relative amplitude of fluctuation (in percent).

TABLE 4
NTTS EXTINCTION FROM THE LITERATURE

ID ^a (1)	Type (2)	Template (3)	W94 (4)	W88 (5)	W86 (6)	S89 (7)	C79 (8)
7.....	K3	N2				2.04	
10.....	K3	N2				0.0	0.03
11.....	K7	N2		0.0			
13.....	K7	...		1.2	1.33	1.25	
16.....	G5	N1				0.57	
20.....	K1	N1		0.1		0.0	
21.....	M0	N2				1.08	0.82
22.....	K2	N2				0.52	0.2
24.....	K5	N2		0.2		0.15	
26.....	K7	N2		0.0		0.0	
27.....	K7,M0	N1		0.3	0.53	0.61	
28.....	K7,M0	...		0.4	0.53		
34.....	K7,M0	N1		0.4	0.31	0.42	
50.....	K0	N2		0.0			
75.....	K1	...					0.08
81.....	K2	...					0.32
168.....	G2	N1	0.2				
176.....	K1	N2	0.2				
177.....	K5	N2	0.2				
179.....	K2	...	0.8				
189.....	K1	N2			0.93		
190.....	K0	N1	1.3			0.87	
191.....	G0	N1	0.6				
220.....	K0,2	N1			0.84		
223.....	G8	...			0.16		

^a Identification number from col. (1) of Table 1.

REFERENCES.—(W94) Walter et al. 1994; (W88) Walter et al. 1988; (W86) Walter 1986; (S89) Strom et al. 1989; (C79) Cohen & Kuh 1979.

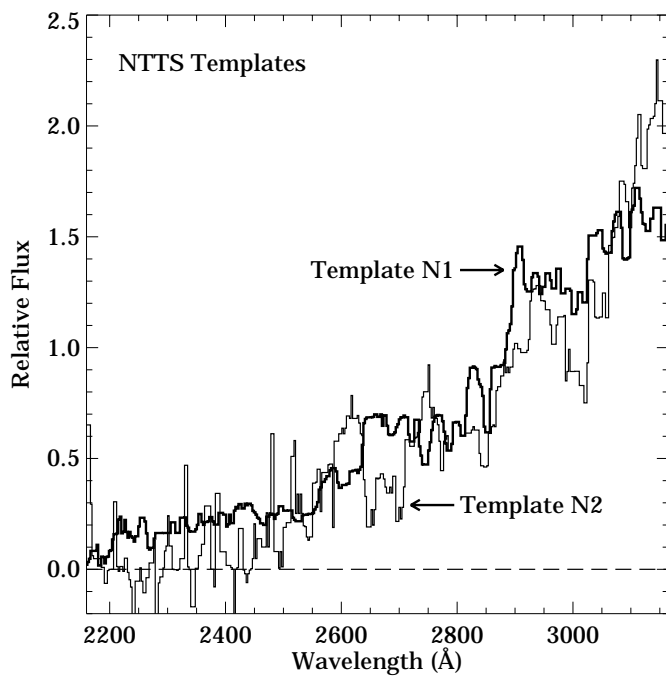


FIG. 3.—Generic NTTS templates used when fitting each co-added CTTS spectrum. Each template spectrum was constructed from co-added spectra of several NTTS with similar spectral features. A 5 pixel wide median filter was applied to suppress noise.

observations with spectral classes in the ranges O3–O9, B0–B2, B3–B5, B6–B9, A0–A3, A4–A9, F0–F2, and F3–F5 and corresponding object classes of 12, 20, 21, 22, 30, 21, 40, and 41. We matched only spectral types with luminosity class V and integer spectral subclass. No F1 V stars matched our search criteria. A secondary search based on right ascensions and declinations robustly yielded the number of LW spectra available for each potential template. For each spectral subclass, we selected a single template with numerous LW observations and a relatively low A_V value in Neckel, Klare, & Sarcander (1980), rejecting any candidate with spectral anomalies.

Table 7 describes our final set of main-sequence templates. The first four columns give the Henry Draper

TABLE 5
SPECTRAL LINE WINDOWS

Ion (1)	Beginning Wavelength (Å) (2)	Ending Wavelength (Å) (3)	TTS Label (4)	HAEBE Star Label (5)
C II].....	2315	2345	“2330 Å”	“2379 Å”
Fe II.....	2345	2440	“2392 Å”	“2379 Å”
Fe II.....	2496	2520	“2508 Å”	...
Fe II.....	2560	2640	“2600 Å”	“2600 Å”
Fe II.....	2720	2766	“2742 Å”	“2742 Å”
Mg II	2775	2822	“2798 Å”	“2798 Å”
Fe II.....	2916	2995	“2955 Å”	...

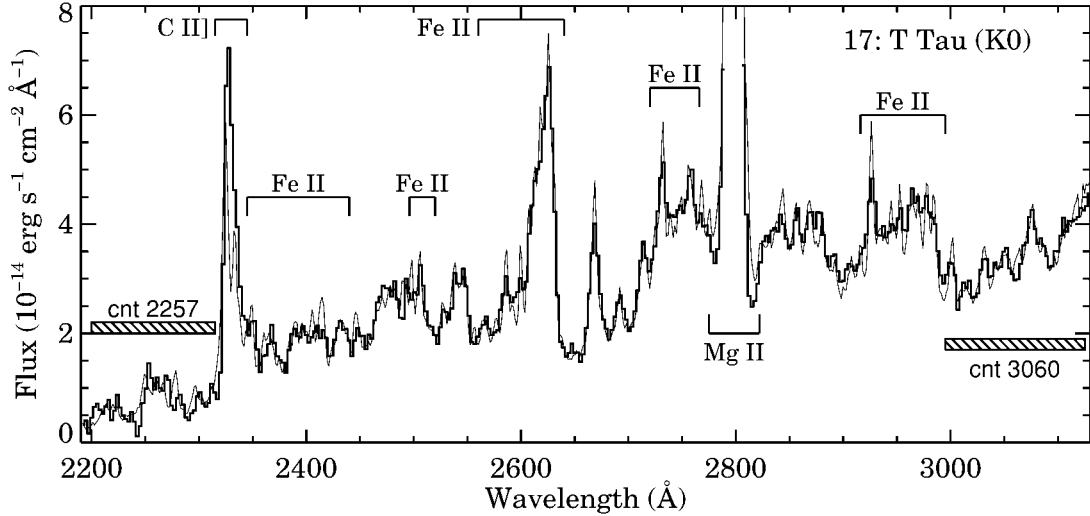


Fig. 4.—Combined *IUE* LW spectrum (dark histogram) of a CTTS with wavelength intervals of interest marked and identified. The superposed STIS spectrum (light curve) matches well after being degraded to a resolution of 6 Å.

(HD) catalog number, the spectral type, the number of useful *IUE* spectra, and A_V from Neckel et al. (1980). Column (5) tabulates 3000 Å minus V band intrinsic color as a function of spectral class, calculated as follows. Using co-added *IUE* spectra with the effects of extinction removed (see below), we measured the unweighted mean flux in a 60 Å wide window centered at 3000 Å, obtaining f_{3000} . We converted these unreddened fluxes to magnitudes, initially adopting a magnitude zero flux of $F_{3000} = 2.79 \times 10^{-9}$ erg s $^{-1}$ cm $^{-2}$ Å $^{-1}$, which is the measured value of f_{3000} for HD 172167 (A0 V, Vega). With V -band magnitudes from the *IUE* merged log and A_V from Table 7, we calculated initial

values of 3000 Å minus V band intrinsic color using the relationship

$$(3000-V)_0 = -2.5 \log \left(\frac{f_{3000}}{F_{3000}} \right) - V + A_V. \quad (1)$$

We then smoothed the $(3000-V)_0$ sequence with a boxcar filter five spectral subclasses wide to suppress scatter of 0.12 mag about the smoothed relationship. Setting $(3000-V)_0 = 0$ at spectral type A0 V, we obtained a refined magnitude zero flux of $F_{3000} = 3.48 \times 10^{-9}$ erg s $^{-1}$ cm $^{-2}$ Å $^{-1}$. Table 7 gives smoothed values of $(3000-V)_0$ based on this normalization. By empirically determining F_{3000} from *IUE* data, we partially compensate for any errors in our adopted values of V , A_V , and the *IUE* flux calibration at 3000 Å.

Using software and procedures described in § 2.2, we combined 463 *IUE* LW observations to produce a single co-added spectrum for each main-sequence template. As indicated in column (3) of Table 7, templates had from 1 to 303 useful spectra, with a median of three useful spectra per template. We removed the effects of continuous extinction using relations in Cardelli et al. (1989) and values of A_V from Table 7. Finally, template spectra were renormalized to obtain a mean of unity in the wavelength interval 1900–3200 Å. For spectral class F1 we averaged the F0 and F2 template spectra. Figure 6 shows all the co-added main-sequence templates. Weak interstellar or circumstellar line absorption is visible in some hot stars, and photospheric absorption becomes prominent at later spectral types.

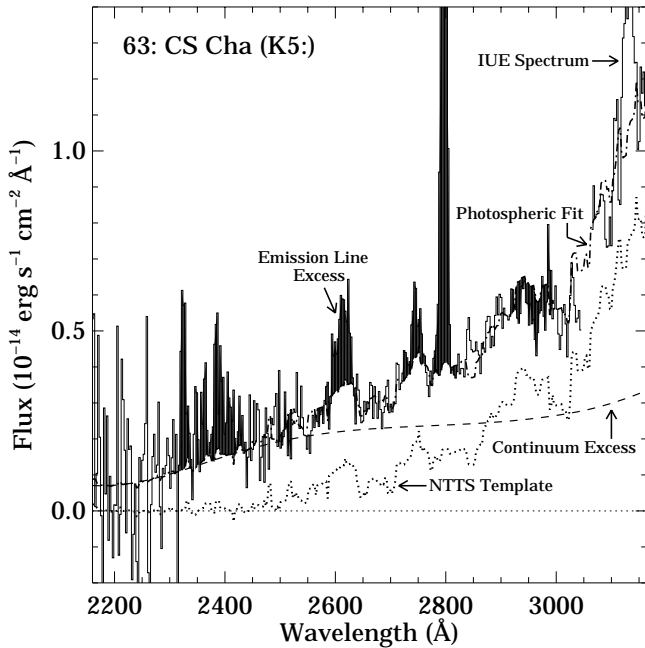


Fig. 5.—Example of the fitting procedure used to model CTTS continua. An NTTS template is combined with a quadratic proxy for the veiling continuum and then scaled and reddened. The shaded areas between the fitted continuum and the observed CTTS spectrum yield integrated line fluxes.

3.4. Extinction toward HAEBE Stars

Assuming LW spectra of HAEBE stars are not significantly veiled by excess continuum from accretion processes, extinction can be determined by fitting spectra of HAEBE stars with reddened template spectra of the main-sequence analogs. Because circumstellar absorption is apparent in spectra of some HAEBE stars (see Fig. 2), we restricted template fits to wavelength intervals that are relatively free of strong circumstellar lines, specifically 1900–2315, 2500–2590, 2650–2700, and 2915–3200 Å. Occasionally we

TABLE 6
MEASURED FLUXES FOR TTS

ID (1)	log cnt2257 (2)	log cnt3060 (3)	C II] 2330 Å (10 ⁻¹³) (4)	Fe II 2392 Å (10 ⁻¹³) (5)	Fe II 2508 Å (10 ⁻¹³) (6)	Fe II 2600 Å (10 ⁻¹³) (7)	Fe II 2742 Å (10 ⁻¹³) (8)	Mg II 2798 Å (10 ⁻¹³) (9)	Fe II 2955 Å (10 ⁻¹³) (10)
3.....	-13.956(86)	-13.569(12)	<0.69	0.90(44)	0.88(16)	-1.28(23)	-0.78(15)	16.01(31)	2.38(24)
7.....	-14.99(46)	-14.292(28)	<0.36	<0.42	<0.11	0.157(73)	<0.097	2.521(83)	<0.17
8.....	-14.76(16)	-14.315(21)	0.67(12)	<0.29	<0.092	0.192(72)	0.115(47)	1.188(78)	-0.181(61)
9.....	<-15.3	-14.828(53)	0.320(88)	<0.22	0.073(32)	0.231(88)	0.136(49)	3.168(45)	<0.093
10.....	<-15.2	-14.031(14)	<0.24	1.32(15)	0.128(46)	0.668(74)	<0.097	3.036(67)	0.485(83)
11.....	-15.01(32)	-14.493(35)	<0.23	<0.30	<0.090	0.40(13)	<0.26	1.114(90)	0.229(67)
12.....	-14.104(12)	-13.7400(20)	1.226(42)	1.313(56)	0.243(20)	2.559(82)	1.229(60)	12.300(52)	0.873(71)
13.....	<-15.3	-15.25(26)	<0.21	<0.30	<0.096	<0.13	<0.083	0.356(45)	<0.17
14.....	-14.524(66)	-14.153(11)	0.898(86)	1.04(11)	0.116(38)	2.354(65)	1.095(40)	9.16(16)	0.947(52)
15.....	-14.255(42)	-13.2829(20)	2.698(99)	3.18(12)	0.755(41)	3.624(63)	2.049(43)	27.96(12)	1.129(71)
16.....	-13.893(74)	-12.8584(52)	<0.81	<1.1	<0.40	<0.65	<0.48	2.68(28)	<1.0
17.....	-14.202(25)	-13.3997(40)	6.65(13)	3.42(14)	0.856(63)	5.06(13)	5.640(100)	42.93(42)	4.51(13)
18.....	-14.518(26)	-13.9123(32)	2.395(47)	0.157(46)	<0.035	0.659(89)	0.267(47)	5.197(45)	0.214(38)
19.....	-14.766(79)	-13.8160(56)	1.418(65)	0.728(86)	0.763(35)	<0.27	<0.15	11.31(10)	0.690(61)
20.....	-14.23(14)	-13.2689(67)	<0.60	<0.76	0.31(12)	2.21(21)	1.11(14)	1.59(14)	1.91(28)
21.....	<-15.2	-15.13(11)	<0.24	<0.27(13)	<0.062	0.436(43)	0.261(27)	0.529(39)	<0.088
22.....	-15.03(42)	-14.005(15)	0.35(15)	0.69(20)	<0.13	<0.17	0.335(53)	0.879(57)	0.525(94)
23.....	-14.90(16)	-14.668(30)	<0.14	<0.18	<0.059	0.448(87)	0.478(30)	2.745(49)	0.349(45)
24.....	<-15.3	-14.785(58)	<0.20	<0.25	<0.073	<0.17	<0.12	0.297(46)	0.220(52)
26.....	<-15.4	-14.716(45)	<0.15	<0.19	<0.057	0.248(67)	0.161(56)	0.487(47)	<0.089
27.....	<-15.6	-14.757(30)	0.152(56)	<0.15	<0.045	0.194(67)	0.144(52)	0.699(41)	<0.19
29.....	-14.388(52)	-13.9919(76)	0.946(85)	1.36(11)	0.484(46)	2.53(26)	1.91(11)	11.70(29)	2.051(93)
31.....	-14.64(16)	-14.147(18)	1.30(15)	1.05(18)	0.442(63)	0.807(84)	0.494(56)	5.52(14)	0.545(81)
33.....	<-15.0	-14.284(36)	<0.40	<0.49	<0.16	1.36(12)	0.428(69)	3.77(10)	<0.22
34.....	<-15.6	-14.788(30)	<0.10	0.537(71)	-0.044(21)	0.229(57)	<0.076	0.793(29)	0.113(30)
35.....	-14.79(25)	-14.269(26)	<0.30	<0.40	<0.14	<0.18	<0.11	1.351(81)	<0.17
36.....	-15.24(43)	-14.464(26)	<0.19	<0.26	<0.076	0.173(56)	0.269(36)	1.604(64)	0.133(56)
37.....	-15.10(19)	-14.348(12)	0.165(58)	0.201(72)	0.128(23)	0.154(47)	<0.046	2.724(43)	0.243(34)
40.....	-14.95(17)	-14.432(24)	0.690(83)	0.74(11)	0.114(35)	0.246(98)	0.275(60)	1.529(42)	0.274(73)
41.....	-15.15(14)	-14.549(14)	0.334(42)	0.644(54)	0.076(17)	0.765(27)	0.422(17)	1.943(27)	0.216(24)
44.....	-14.07(49)	-14.58(38)	<3.0	4.2(2.0)	<1.1	<1.5	<0.76	2.84(39)	1.85(52)
45.....	<-15.3	-14.923(71)	-0.253(88)	<0.22	<0.069	0.309(49)	<0.058	0.863(37)	<0.095
46.....	-13.889(13)	-13.2611(16)	-0.59(12)	-6.02(28)	0.680(90)	-6.11(46)	-3.23(21)	6.366(93)	1.18(20)
47.....	-14.087(38)	-13.6842(69)	0.44(13)	-0.86(16)	0.333(69)	0.79(10)	0.172(62)	5.591(98)	-0.704(93)
48.....	-14.428(83)	-13.8834(97)	0.80(13)	<0.33	<0.12	<0.18	0.339(62)	6.46(30)	0.475(83)
49.....	-14.91(15)	-14.184(14)	0.662(85)	1.03(11)	0.149(37)	1.381(59)	0.555(38)	4.643(75)	<0.11
50.....	<-15.0	-13.837(14)	0.67(19)	1.66(24)	<0.19	-0.37(11)	-0.538(69)	1.348(86)	-0.28(13)
52.....	-14.068(36)	-12.9209(22)	1.25(13)	-1.49(18)	0.198(66)	-0.45(11)	<0.16	9.60(12)	-0.52(18)
55.....	-12.792(22)	-12.649(14)	-5.7(1.8)	-13.0(2.9)	<2.9	<4.9	5.9(1.9)	<3.7	<5.1
56.....	-13.470(12)	-13.0151(32)	4.87(21)	-1.43(28)	2.57(14)	1.51(21)	1.23(15)	113.11(88)	1.81(23)
59.....	-14.64(48)	-13.342(22)	1.81(55)	<1.4	<0.50	0.88(39)	-0.67(31)	8.71(40)	<1.2
61.....	-14.102(34)	-13.1098(49)	1.77(14)	<0.39	0.92(22)	<2.8	<1.7	20.10(53)	3.77(30)
62.....	<-14.2	-14.17(28)	<2.8	<3.9	<1.3	<1.8	<1.1	7.76(72)	<2.0
64.....	-13.074(41)	-11.9663(25)	<2.8	12.2(2.1)	-3.54(67)	33.6(1.3)	25.43(94)	73.2(1.2)	10.2(2.0)
66.....	-14.39(44)	-14.41(13)	<1.3	<1.7	-0.50(25)	-0.84(33)	<0.39	1.61(21)	<0.58
67.....	-13.98(16)	-13.1135(72)	<1.2	<1.6	<0.48	2.96(40)	1.07(23)	5.52(29)	<0.88
68.....	-14.30(19)	-13.676(32)	<0.92	-2.54(61)	<0.45	<1.6	<1.3	9.53(52)	1.86(42)
69.....	<-14.5	-13.827(33)	1.54(61)	<1.5	<0.51	<0.65	0.79(20)	5.77(35)	<0.58
81.....	-13.90(28)	-13.596(23)	<2.7	4.9(1.7)	<0.71	2.05(46)	1.37(25)	3.34(28)	<0.76
96.....	-13.068(17)	-12.7643(69)	<1.2	-8.24(83)	1.70(35)	<1.2	-3.93(45)	3.57(54)	-5.23(84)
97.....	<-14.8	-14.40(12)	<0.87	1.49(60)	<0.45	<0.59	<0.37	1.73(21)	0.58(28)
102.....	<-14.6	-14.067(84)	<1.0	<1.5	<0.51	<0.73	<0.46	2.49(24)	1.76(40)
104.....	-14.22(26)	-13.276(22)	<1.4	<2.2	<0.71	<1.1	<0.78	7.70(54)	2.49(75)
105.....	<-14.1	-13.552(39)	<3.4	<4.6	<1.3	2.53(91)	<0.96	1.59(51)	<1.4
112.....	-14.52(48)	-14.005(84)	<1.4	-2.09(90)	<0.65	-1.48(47)	-0.92(34)	4.35(39)	1.84(53)
114.....	-14.599(87)	-13.4769(36)	0.480(92)	<0.22	0.709(45)	0.596(62)	<0.084	10.48(14)	-1.542(81)
115.....	-14.53(26)	-13.503(10)	<0.58	<0.84	<0.24	1.75(17)	0.582(99)	1.80(12)	<0.42
124.....	<-14.5	-13.736(64)	<1.3	<2.0	<0.70	-1.86(72)	-1.17(57)	-1.54(48)	3.43(63)
126.....	<-14.5	-13.776(66)	<1.5	<2.0	<0.75	<1.1	<0.69	<0.74	1.72(67)
140.....	-14.87(32)	-14.428(30)	<0.35	0.96(28)	0.202(65)	0.561(73)	0.344(45)	1.737(57)	<0.16
141.....	-14.77(20)	-14.284(21)	<0.24	-0.56(15)	<0.12	<0.21	-0.181(64)	2.762(66)	<0.14
142.....	<-15.4	-14.162(13)	0.557(83)	0.840(99)	<0.084	<0.65	<0.47	1.59(18)	0.699(67)
143.....	-13.585(20)	-13.3706(73)	5.12(29)	8.81(40)	1.05(15)	9.64(25)	5.62(17)	32.33(51)	0.45(21)

TABLE 6—Continued

ID (1)	log cnt2257 (2)	log cnt3060 (3)	C II] 2330 Å (10 ⁻¹³) (4)	Fe II 2392 Å (10 ⁻¹³) (5)	Fe II 2508 Å (10 ⁻¹³) (6)	Fe II 2600 Å (10 ⁻¹³) (7)	Fe II 2742 Å (10 ⁻¹³) (8)	Mg II 2798 Å (10 ⁻¹³) (9)	Fe II 2955 Å (10 ⁻¹³) (10)
145	-15.03(31)	-14.124(18)	0.58(12)	1.23(16)	<0.098	0.619(78)	0.365(46)	2.96(20)	-0.297(68)
146	<-14.4	-14.80(36)	<1.6	<2.0	<0.61	1.23(41)	<0.46	4.30(35)	<0.65
148	-14.95(45)	-13.795(14)	<0.34	<0.44	<0.13	0.39(10)	0.424(76)	1.474(98)	<0.28
149	-14.68(13)	-14.254(16)	0.244(100)	<0.25	0.148(44)	<0.12	<0.075	2.542(56)	0.237(55)
151	-14.62(44)	-14.125(28)	<0.84	1.21(50)	0.27(13)	0.48(14)	0.193(78)	0.982(91)	0.31(13)
152	<-14.5	-14.48(11)	-1.66(69)	<1.7	<0.48	0.57(25)	<0.27	2.26(23)	0.85(21)
153	-14.34(19)	-13.399(14)	2.46(40)	3.89(60)	1.08(25)	<0.74	0.89(25)	22.48(63)	4.59(39)
163	<-15.5	-15.164(69)	<0.11	0.175(76)	<0.053	<0.063	<0.036	0.544(23)	<0.055
164	-15.10(42)	-13.906(10)	0.71(13)	0.40(16)	<0.10	<0.15	<0.099	5.50(12)	0.279(83)
165	<-15.2	-14.954(74)	0.210(99)	<0.28	0.142(39)	0.593(94)	0.195(36)	0.787(47)	0.216(48)
167	-14.96(24)	-14.496(28)	0.79(11)	0.41(13)	<0.084	0.330(97)	<0.12	1.496(46)	<0.12
168	-13.350(71)	-12.5186(60)	<2.2	-4.9(1.6)	<1.1	<2.0	<1.4	<1.4	<2.6
169	<-15.1	-14.95(10)	<0.28	<0.36	<0.13	<0.15	<0.085	0.634(62)	<0.14
170	-13.1455(89)	-12.8304(22)	2.93(30)	-13.83(42)	1.83(20)	-13.11(29)	-3.63(20)	56.98(61)	15.07(27)
172	<-14.6	-14.292(82)	<0.92	<1.4	<0.43	1.56(30)	<0.34	5.53(87)	-0.56(27)
173	-14.28(19)	-13.1125(69)	<0.73	1.72(52)	0.44(18)	2.93(30)	0.90(20)	1.88(21)	0.79(35)
174	-14.59(18)	-14.262(27)	<0.41	<0.47	0.257(97)	1.20(15)	0.214(74)	1.724(88)	<0.22
175	<-15.0	-13.685(20)	0.78(23)	<0.62	<0.22	0.39(16)	0.55(11)	1.67(12)	1.20(25)
176	<-15.1	-14.109(19)	0.36(16)	1.11(22)	0.243(70)	0.333(96)	0.153(53)	0.853(59)	<0.18
177	-14.79(31)	-14.129(49)	<0.37	<0.48	<0.16	<0.32	<0.26	1.12(19)	0.55(27)
178	<-14.8	-14.38(12)	<0.80	2.30(59)	0.96(23)	1.00(30)	0.89(19)	3.61(23)	<0.58
180	-13.941(62)	-13.669(11)	2.28(33)	1.30(44)	<0.33	<0.50	0.64(13)	2.85(18)	<0.34
182	<-15.1	-15.13(17)	0.44(14)	<0.36	<0.14	0.45(11)	0.198(53)	0.847(71)	0.750(76)
183	-14.140(72)	-13.682(10)	1.18(20)	<0.55	1.07(11)	-0.41(14)	-0.508(88)	4.98(12)	1.29(14)
188	<-15.2	-13.980(29)	<0.31	0.85(23)	<0.17	0.52(15)	0.67(10)	3.46(17)	0.61(20)
189	<-14.8	-14.344(53)	<0.59	<0.75	<0.23	-0.83(15)	<0.19	<0.23	<0.29
190	<-15.0	-14.068(27)	<0.44	0.78(30)	0.35(10)	0.61(15)	0.236(87)	1.492(97)	0.43(14)
191	-14.237(87)	-13.1172(43)	-0.55(18)	-0.76(25)	<0.20	<0.35	<0.25	-1.41(12)	-1.77(24)
192	-14.80(27)	-14.429(29)	0.56(15)	1.05(21)	0.201(66)	<0.15	-0.099(44)	2.780(69)	<0.13
194	<-15.1	-14.437(31)	<0.32	2.04(25)	<0.14	0.59(11)	0.205(71)	2.81(13)	0.59(11)
199	<-15.0	-13.819(13)	0.78(21)	1.21(28)	<0.18	1.52(15)	0.78(12)	4.90(14)	0.45(15)
200	<-14.8	-14.086(50)	<0.55	<0.81	<0.32	<0.47	<0.42	1.62(42)	1.26(36)
201	-14.92(26)	-14.185(20)	0.38(12)	0.75(16)	0.112(52)	0.345(79)	0.405(52)	2.667(84)	0.268(81)
202	<-14.9	-14.358(37)	0.77(23)	0.69(31)	0.206(96)	0.41(11)	0.36(15)	3.12(11)	0.61(12)
204	-14.64(18)	-14.892(83)	<0.27	<0.34	<0.10	0.174(70)	-0.103(39)	<0.11	<0.14
206	-14.46(12)	-13.857(21)	0.48(21)	<0.57	0.33(11)	2.41(35)	2.04(21)	15.08(39)	2.10(21)
207	-13.322(33)	-12.5433(34)	<1.3	-9.23(86)	<0.57	-7.29(45)	-4.96(33)	22.66(53)	-12.06(79)
216	-14.50(11)	-13.8130(91)	1.16(15)	1.69(19)	0.243(61)	1.301(88)	0.578(57)	4.430(86)	0.307(91)
217	<-14.8	-13.917(25)	2.12(32)	3.70(48)	<0.34	3.47(24)	2.48(14)	12.40(34)	<0.41
219	-13.968(53)	-13.274(14)	1.36(29)	-3.75(41)	1.10(22)	-2.81(34)	-2.48(30)	2.91(31)	<1.1
220	-14.76(26)	-14.152(25)	<0.34	<0.43	<0.10	0.517(80)	0.306(54)	0.762(74)	<0.20
230	<-15.3	-14.232(29)	<0.25	<0.34	0.316(61)	0.454(81)	<0.11	5.07(14)	-0.468(97)
236	-13.928(32)	-13.2713(79)	0.90(19)	-2.58(27)	1.89(15)	-4.29(47)	-1.60(25)	6.58(41)	3.53(35)
238	-15.06(31)	-14.482(30)	0.72(11)	0.36(14)	<0.10	0.79(12)	0.750(69)	5.77(14)	0.474(61)

NOTES.—Values in each column must be multiplied by the factor at the top of each column. Continuum spectral fluxes are in units of ergs s⁻¹ cm⁻² Å⁻¹. Integrated line fluxes are in units of ergs s⁻¹ cm⁻². Uncertainties in the last two digits are enclosed in parentheses after each value. Tabulated upper limits are twice the measured uncertainty. Line fluxes in several columns include significant contributions from more than one species. Table 6 is also available in machine-readable form in the electronic edition of the *Astrophysical Journal Supplement*.

excluded additional wavelength intervals contaminated by spectral features not in the templates. For HAEBE stars with half-integer spectral subclasses, we interpolated between neighboring template spectra described in § 3.3. When fitting spectra of HAEBE stars, the only free parameters were A_V and a global scale factor, which accounts for distance and radius differences between the template and HAEBE star.

Table 8 presents our values of A_V for HAEBE stars, which are ordered by identification number from Table 1. Column (2) contains the spectral class of the main-sequence template that yielded the best fit, whenever a change from the literature value in Table 1 was required.

Column (4) gives A_V values obtained by fitting IUE LW spectra with the most appropriate template. Columns (3) and (5) give A_V values when the template spectral class is increased (A_V^{+2}) or decreased (A_V^{-2}) by two subclasses. We do not report formal uncertainties in A_V because systematic errors are larger. Potential errors in A_V are best assessed by noting the range of values obtained with modest changes in template spectral class. Earlier than spectral class B5, LW template characteristics change more slowly with spectral class, so A_V is less sensitive to a change of two subclasses.

The analysis presented here assumes a typical interstellar value of 3.1 for the ratio of total to selective extinction,

TABLE 7
MAIN-SEQUENCE TEMPLATE STARS

HD (1)	Spectral Type (2)	N_{IUE} (3)	A_V^a (4)	$(3000-V)_0$ (5)
303308	O3 V	4	1.09	-2.13
164794	O4 V	3	1.13	-2.36
93204	O5 V	2	1.36	-2.33
199579	O6 V	4	1.19	-2.36
48099	O7 V	3	0.91	-2.29
97848	O8 V	1	0.94	-2.21
93521	O9 V	303	0.00	-2.16
46106	B0 V	1	1.33	-2.05
144470	B1 V	1	0.75	-1.84
37776	B2 V	5	0.36	-1.75
120315	B3 V	52	0.10	-1.59
136664	B4 V	2	0.08	-1.37
25340	B5 V	5	0.08	-1.16
90994	B6 V	3	0.07	-0.98
87901	B7 V	8	0.08	-0.69
196519	B8 V	11	0.19	-0.39
98664	B9 V	5	0.10	-0.21
172167	A0 V	13	0.01	0.00
41695	A1 V	2	0.11	0.08
97633	A2 V	1	-0.16	0.18
102647	A3 V	7	0.04	0.23
13041	A4 V	1	-0.04	0.35
11636	A5 V	7	-0.06	0.36
28527	A6 V	2	-0.03	0.48
87696	A7 V	1	-0.02	0.52
28910	A8 V	6	-0.08	0.51
157792	A9 V	1	0.08	0.50
29375	F0 V	2	0.27	0.54
164259	F2 V	2	0.02	0.52
157950	F3 V	1	0.06	0.58
8799	F4 V	2	0.08	0.60
111456	F5 V	2	0.05	0.68

^a Visual extinction from Neckel et al. 1980.

$R_V = A_V/E(B-V)$. Larger values of R_V may be more appropriate for some HAEBE stars, especially when the star is dimmer than usual (Thé et al. 1996). On the other hand, Thé et al. (1996) find for HR 5999 that extinction anomalies in the UV ($3.3 < R_V < 3.9$) are less pronounced than in the optical and IR ($R_V > 5.8$). For the sake of expediency, we simply adopted the value $R_V = 3.1$ throughout our analysis.

For some HAEBE stars, our template fitting procedure yielded unusually large visual extinctions, notably $A_V = 6.25$ for R CrA (A5, no. 222). As a consistency check, we also determined values of A_V from observed $E(3000-V)$ color excess, relative to the intrinsic values reported in column (5) of Table 7. We computed $3000-V$ color using the procedure described in § 3.3, except that we used $A_V = 0$ to obtain observed rather than intrinsic colors and we adopted V -band magnitudes directly from the source catalogs cited in § 2.1. Column (6) of Table 8 lists our measured values of $3000-V$ color from which $E(3000-V)$ may be calculated. Assuming V -band photometry has an effective wavelength of 5500 Å, the extinction law of Cardelli et al. (1989) implies $A_V = 1.21 E(3000-V)$. Column (7) of Table 8 gives values of A_V calculated from this relationship and $E(3000-V)$ color excess.

Figure 7 compares our values of A_V measured via main-sequence template fitting and $E(3000-V)$ color excess. The

median of differences between the two measures is 0.09 mag, while the median of the absolute values of the differences is 0.39 mag. These statistics provide robust estimates of the systematic and random differences between the two measurement techniques. Outliers such as VV Ser (A0, no. 218), which is a member of the UX Ori class, are likely affected by interesting circumstellar processes that are beyond the scope of this study.

3.5. Continuum and Excess Line Emission from HAEBE Stars

For each co-added spectrum of a HAEBE star, we calculated the mean continuum flux per Å in the same two wavelength intervals used in § 3.2 for CTTS. Columns (2) and (3) of Table 9 presents logarithms of our measured fluxes. Throughout the table, parentheses enclose the formal uncertainty in the two least significant digits, unless a 2σ upper limit is quoted. Figure 8 shows part of our co-added spectrum of the HAEBE star HD 163296 (A1, no. 215), along with an entire STIS E230M spectrum (data set o66q01020) degraded to 6 Å resolution and multiplied by a polynomial to match the observed IUE continuum. The pseudo-continuum window at 3060 Å does contain contributions from photospheric and perhaps circumstellar lines but is still relatively free of line absorption.

In principle circumstellar material associated with HAEBE stars may affect the apparent strengths of normal photospheric lines. Conversely, anomalous line strengths may provide a diagnostic for evaluating the status of candidate HAEBE stars. To provide quantitative data for exploring this possibility, we measured *excess* line emission in each co-added IUE spectrum of a HAEBE star. We define excess emission or absorption as a localized deviation from unity after division by a fitted main-sequence template (see § 3.4).

Template division removes the photospheric contribution to spectral lines, leaving residuals that are mainly due to circumstellar absorption and perhaps accretion. Before measuring localized excesses, division by a fourth-order polynomial is used to iteratively remove global residuals that are typically small. Then we simply average deviations from unity in the spectral line windows defined below. Thus, our line excess measures the fractional change in line depth relative to line depth in a main-sequence analog. Positive values imply excess emission, while negative values imply extra absorption. We computed formal uncertainties for each excess by propagating uncertainties in spectrum points used to construct the excess. We then added an additional 3% uncertainty in quadrature to crudely account for residual errors in continuum normalization, determined by visual inspection. This 3% minimum uncertainty is not normally distributed and frequently dominates the final uncertainty.

As illustrated in Figure 8, individual spectral lines are usually blended in low-resolution IUE spectra, so we measured mean excesses in broad spectral windows typically dominated by lines of a single ion. Specifically, we use the wavelength intervals with a label in column (5) of Table 5. Note that the first two spectral windows used for CTTS are merged into a single “2379 Å” window for HAEBE stars because Fe II dominates both windows. These line windows are illustrated graphically in Figure 8.

Columns (4) through (7) of Table 9 present our measurements of excess line emission (positive values) or absorption

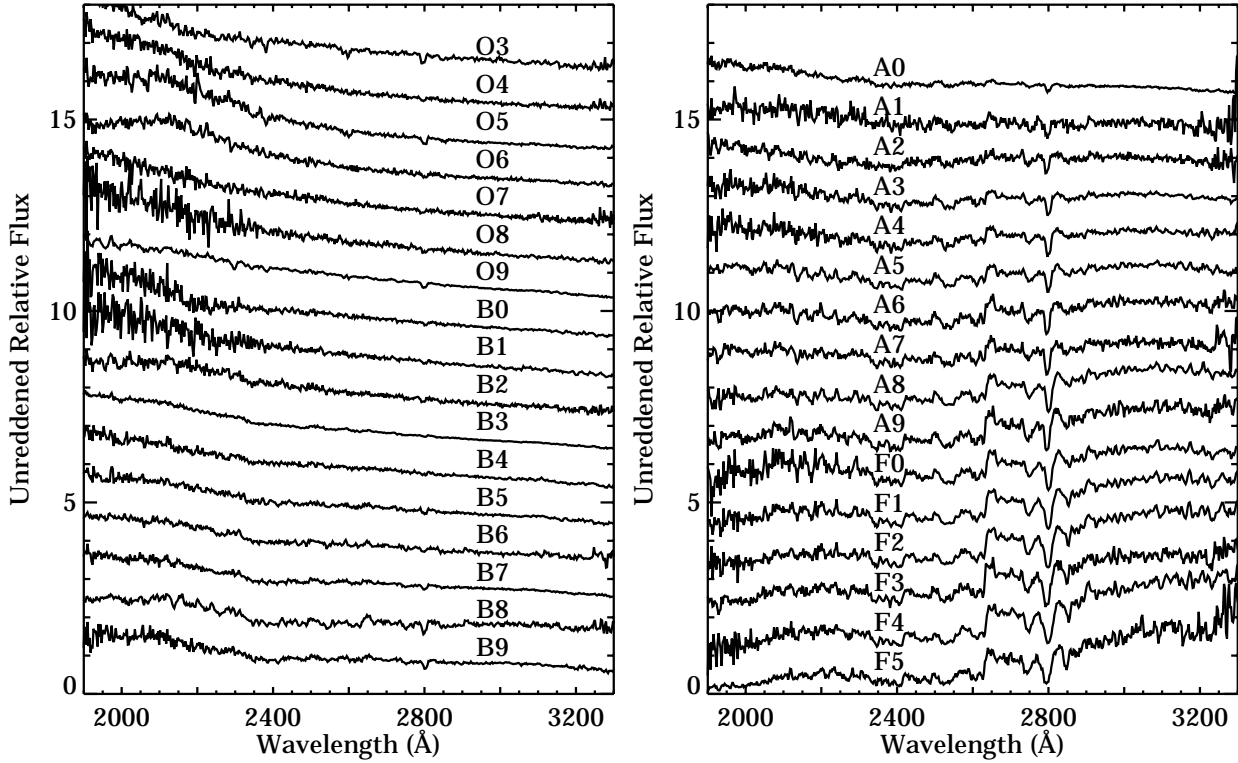


FIG. 6.—Co-added *IUE* spectra of main-sequence templates used as proxies for photospheric spectra of HAEBE stars. Mean flux has been normalized to unity and then offset for presentation purposes. Note the onset of prominent line absorption at later spectral types. Spectral class labels may be used as an index into Table 7.

(negative values) in each star. For a few cool or highly reddened stars, excesses are not reported at the shortest wavelengths due to insignificant flux in either the template or the

HAEBE star. A trailing colon indicates measurements that may be compromised by unusually large systematic errors. Despite the limitations imposed by low resolution, these excess measurements are potentially useful for studying peculiarities of HAEBE stars and for planning more detailed observational studies.

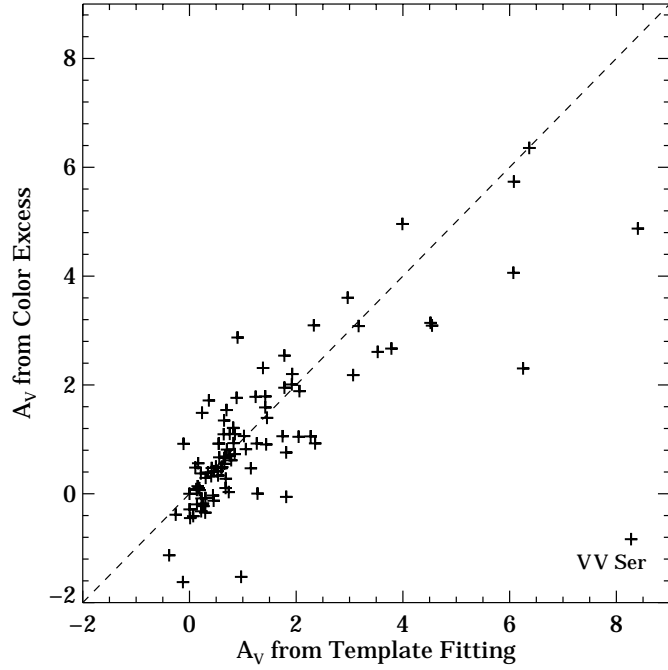


FIG. 7.—Comparison of A_V values for HAEBE stars, based of $E(3000 - V)$ color excess and on fits of *IUE* LW spectra with main-sequence templates. The two methods generally agree, but with a median scatter of 0.4 mag. VV Ser is an extreme outlier.

4. DISCUSSION

As mentioned in § 1, the *IUE* final archive contains many more UV spectra of PMS stars than all other mission archives combined. In particular, for the 238 stars in Table 1, we searched the *HST* archive for UV spectra obtained with either the Goddard High Resolution Spectrograph (GHRS) or Space Telescope Imaging Spectrograph (STIS). Tables 10 and 11 break down the number of PMS sources observed by instrument and category. *HST* spectra are better resolved and less noisy than *IUE* spectra, but in several cases the *HST* spectra also have more limited wavelength coverage. *IUE* has observed more PMS sources than *HST* by a factor of at least 2 for TTS and 10 for HAEBE stars. It is unlikely that *HST* will ever observe all of the PMS stars observed by *IUE*, so the *IUE* archive will remain a valuable resource for years to come.

As in Paper I, we find that data quality in the *IUE* final archive (Nichols & Linsky 1996) is generally excellent. NEWSIPS processing is definitely superior to the original IUESIPS processing. In particular, reduced pattern noise increases the value of co-adding multiple spectra of the same source, as we have done here. Even final archive spectra may have flaws, as indicated by the status codes described in the Appendix. For this reason, it is still important to visually

TABLE 8
EXTINCTION OF HAEBE STARS

ID ^b	Template ^a Class	LW A_V^{+2}	LW A_V	LW A_V^{-2}	(3000– V)	$E(3000-V)$
(1)	(2)	(3)	(4)	(5)	(6)	(7)
1.....	...	1.74	2.05	2.60	1.00	1.05
2.....	...	1.85	2.06	2.19	0.39	1.89
6.....	...	1.88	1.74	2.10	1.24	1.06
42.....	B7	-0.09	0.01	0.15	-1.05	-0.45
43.....	...	2.63	3.07	3.34	2.03	2.18
51.....	...	0.34	0.60	0.71	0.28	0.47
53.....	A3	0.33	0.54	0.61	0.51	0.34
54.....	A5	0.38	0.36	0.58	1.78	1.72
57.....	...	1.49	1.42	1.64	-0.80	1.59
58.....	...	1.49	1.28	1.72	0.37	0.00
60.....	A8	0.54	0.35	0.69	0.83	0.39
63.....	...	0.39	0.66	0.80	0.77	0.66
65.....	A4	-0.02	0.17	0.25	0.43	0.11
71.....	...	0.12	0.41	0.55	0.27	0.32
72.....	...	-0.32	-0.26	-0.11	0.05	-0.38
73.....	...	0.50	0.65	0.97	1.29	1.35
74.....	...	-0.14	0.07	0.11	-0.54	-0.41
76.....	...	-0.28	0.00	0.16	-0.23	-0.29
79.....	...	0.00	0.14	0.21	-1.33	-0.19
80.....	...	0.64	0.82	0.74	-0.80	1.21
82.....	O6	0.40	0.70	0.60	-1.69	0.81
84.....	O9	0.54	0.69	0.64	-0.90	1.54
85.....	...	0.45	0.75	0.65	-1.78	0.70
86.....	...	-0.47	-0.38	-0.08	-0.75	-1.13
87.....	...	0.45	0.78	0.90	0.51	0.62
88.....	...	0.26	0.29	0.37	-2.23	-0.35
90.....	B6	0.13	0.30	0.34	-1.04	-0.08
91.....	...	3.60	3.53	4.09	2.66	2.61
92.....	...	0.18	0.11	0.31	-1.71	0.48
93.....	...	0.00	0.16	0.07	-1.38	0.56
95.....	...	0.59	0.75	0.65	-0.94	1.10
98.....	...	0.04	0.15	0.29	-1.47	0.14
99.....	...	0.04	0.24	0.29	1.45	1.49
100.....	...	-0.01	0.13	0.27	-0.32	0.09
101.....	F0	-0.02	0.50	0.30	0.95	0.50
103.....	...	0.82	1.06	1.23	0.76	0.82
106.....	A4	0.29	0.55	0.66	1.11	0.92
107.....	...	-0.42	-0.12	0.02	-1.33	-1.62
108.....	...	4.29	4.52	4.97	2.29	3.14
109.....	...	0.30	0.42	0.56	-1.20	0.47
110.....	B9	1.50	1.78	2.00	1.89	2.54
111.....	...	0.48	0.68	0.74	-0.12	0.11
113.....	A8	0.84	0.65	1.00	0.96	0.55
116.....	B8	0.60	0.74	0.91	-0.37	0.03
117.....	...	-0.30	0.22	0.02	0.27	-0.32
118.....	...	0.52	0.64	0.79	-0.69	1.09
119.....	B9	0.76	0.97	1.04	-1.46	-1.53
120.....	B8	1.31	1.42	1.70	1.08	1.79
121.....	...	0.68	0.83	0.91	-0.40	0.93
122.....	...	4.00	3.99	4.23	2.03	4.96
125.....	...	0.32	0.46	0.62	-0.05	0.42
129.....	B8	0.31	0.45	0.60	-0.50	-0.13
130.....	...	0.54	0.67	0.75	-0.60	0.69
131.....	...	0.65	0.85	0.83	-1.15	0.73
132.....	B5	5.68	6.07	6.27	2.18	4.06
133.....	...	1.75	1.78	1.86	-0.44	1.95
134.....	...	0.02	0.14	0.28	-1.53	0.07
135.....	...	-0.22	-0.11	0.10	1.28	0.92
137.....	B8	2.19	2.27	2.60	0.47	1.05
138.....	...	1.74	1.92	2.04	0.14	2.20
139.....	...	1.61	1.81	1.93	-0.45	0.76
144.....	A3	0.44	0.68	0.78	0.46	0.28
147.....	...	0.78	1.02	1.10	-0.10	1.06

TABLE 8—Continued

ID ^b (1)	Template ^a Class (2)	LW A_V^{+2} (3)	LW A_V (4)	LW A_V^{-2} (5)	(3000– V) (6)	$E(3000-V)$ A_V (7)
150.....	0.56	0.85	0.99	0.90
154.....	0.40	0.61	0.67	0.20
155.....	0.02	0.23	0.27	-0.28
156.....	0.30	0.56	0.68	0.45
157.....	0.23	0.44	0.53	0.32
158.....	0.65	0.82	0.91	-0.17
160.....	B8	1.72	1.81	2.15	-0.44	-0.06
161.....	2.28	2.35	2.75	0.37
162.....	0.52	0.25	0.40	-0.15
166.....	0.01	0.30	0.45	0.24
171.....	A9	0.93	1.15	1.53	0.88	0.47
181.....	A8	0.38	0.21	0.58	0.82	0.37
184.....	0.21	0.55	0.62	1.28
196.....	2.33	2.33	2.50	0.50
205.....	A3	1.14	1.45	1.64	1.38	1.39
208.....	B5	4.15	4.55	4.72	1.38	3.09
209.....	3.51	3.78	3.72	0.40
210.....	0.89	0.90	1.11	2.73
211.....	6.08	6.37	6.31	3.44
213.....	1.43	1.38	1.51	-0.14
214.....	5.89	6.08	6.26	3.05
215.....	A2	0.07	0.19	0.48	0.24	0.07
218.....	8.43	8.28	8.41	-0.69
221.....	0.68	0.88	0.94	1.25
222.....	7.68	6.25	7.35	2.26
224.....	0.27	0.52	0.65	0.24
225.....	A4	0.97	1.26	1.46	1.11	0.92
226.....	A5	0.17	0.26	0.42	0.18	-0.23
227.....	2.97	3.17	3.31	0.87
231.....	1.11	1.24	1.39	-0.12
232.....	1.76	1.92	2.03	-0.02
233.....	2.29	2.97	3.22	1.99
234.....	1.17	1.44	1.56	1.09
237.....	8.23	8.40	8.63	1.97
						4.87

^a Only specified when template spectral class differs from the value in Table 1.

^b Identification number from col. (1) of Table 1.

examine and manually assess spectra prior to co-addition. In some cases, low-resolution spectra extracted with the INES package (Rodríguez-Pascual et al. 1999) are superior to final archive spectra processed with the NEWSIPS package.

The PMS spectral catalogs presented here and in Paper I can be used to motivate and guide further archival analysis or new observations with *HST*. For example, when combining spectra from multiple epochs, we have largely ignored temporal variations, merely noting the presence of significant variability (see Table 3). Detailed analysis of flux variations may provide clues about the physical origin of variability (e.g., Ardila & Basri 2000). In particular, *IUE* LW spectra of HAEBE stars could be used to study how brightness variations affect R_V (e.g., Thé et al. 1996) and strength of the 2200 Å bump. More generally, the mean spectra presented here are affected by many physical processes. Accretion and magnetic activity have similar observational characteristics at this resolution (see Paper II), but extinction and circumstellar absorption can be distinctive.

TABLE 9
CONTINUUM FLUXES AND EXCESS LINE EMISSION FOR HAEBE STARS

ID (1)	log cnt2257 (2)	log cnt3060 (3)	Fe II 2379 Å (4)	Fe II 2600 Å (5)	Fe II 2742 Å (6)	Mg II 2798 Å (7)
1.....	-13.705(55)	-13.2245(98)	<0.09	<0.07	0.07(04)	<0.07
2.....	-13.451(47)	-12.837(11)	-0.15(04)	-0.20(03)	-0.24(03)	0.09(03)
6.....	-13.557(65)	-12.7084(65)	<0.08	<0.07	<0.07	0.38(03)
42.....	-9.9990(62)	-10.2202(47)	<0.06	<0.06	<0.06	<0.06
43.....	<-14.6	-13.426(15)	<0.51	<0.08	<0.08	0.43(04)
51.....	-11.5237(50)	-11.4034(35)	-0.11(03)	-0.16(03)	-0.07(03)	<0.06
53.....	-12.019(12)	-11.7016(93)	-0.12(03)	-0.25(03)	-0.24(03)	0.69(04)
54.....	-13.301(13)	-13.0340(30)	0.06(03)	0.11(03)	0.15(03)	0.50(03)
57.....	-10.8848(74)	-10.5436(41)	<0.06	<0.06	<0.06	<0.06
58.....	-13.328(47)	-12.9086(89)	<0.09	<0.07	<0.07	-0.12(03)
60.....	-12.483(19)	-12.0455(41)	<0.07	<0.06	<0.06	0.25(03)
63.....	-12.269(61)	-11.9940(96)	-0.24(05)	-0.27(03)	-0.21(03)	0.08(03)
65.....	-13.353(20)	-13.3323(76)	1.50(05)	1.24(04)	1.47(05)	0.90(04)
71.....	-11.877(13)	-11.7794(68)	<0.06	<0.06	<0.06	<0.06
72.....	-12.423(11)	-12.4439(39)	0.25(03)	0.11(03):	0.12(03)	0.17(03)
73.....	-13.379(92)	-13.036(30)	<0.13	<0.09	<0.10	0.15(05)
74.....	-11.743(12)	-11.865(14)	<0.06	<0.06	<0.08	<0.07
76.....	-12.348(11)	-12.421(15)	<0.06	<0.06	<0.07	<0.07
79.....	-10.9137(67)	-11.11298(62)	<0.06	<0.06	<0.06	<0.06
80.....	-11.5244(88)	-11.5150(55)	<0.06	<0.06	<0.06	-0.07(03)
82.....	-10.1934(64)	-10.4769(72)	<0.06	<0.06	<0.07	0.12(03)
84.....	-11.1435(20)	-11.2960(16)	<0.07	<0.07	<0.06	<0.06
85.....	-9.5839(56)	-9.8174(59)	<0.06	<0.06	<0.06	0.06(03)
86.....	-12.2528(73)	-12.3777(37)	0.18(03)	<0.06	0.09(03)	0.10(03)
87.....	-12.807(91)	-12.689(14)	<0.11	-0.11(04)	-0.08(03)	-0.10(03)
88.....	-10.0364(75)	-10.2623(91)	<0.06	<0.06	<0.06	<0.07
90.....	-11.803(16)	-11.895(15)	0.07(03)	<0.06	<0.07	<0.07
91.....	-14.100(77)	-13.4703(76)	...	0.24(04)	0.26(04)	0.90(04)
92.....	-9.5178(35)	-9.8242(37)	<0.06	<0.06	<0.06	<0.06
93.....	-9.9789(98)	-10.328(13)	<0.07	<0.07	<0.07	<0.07
95.....	-10.8204(59)	-10.8473(52)	<0.07	<0.06	<0.06	<0.06
98.....	-10.5222(62)	-10.8108(69)	<0.06	<0.06	<0.06	<0.06
99.....	-13.198(20)	-13.018(12)	<0.07	-0.11(03)	<0.06	0.13(03)
100.....	-11.804(16)	-11.953(18)	<0.07	<0.07	<0.07	<0.07
101.....	-13.063(18)	-12.6634(44)	<0.07	<0.06	0.08(03)	0.53(03)
103.....	-13.1674(95)	-12.7547(32)	-0.17(03)	-0.18(03)	-0.15(03)	0.35(04)
106.....	-13.323(20)	-13.0237(44)	0.13(03)	0.11(03)	0.25(03)	0.98(04)
107.....	-11.309(17)	-11.4685(86)	<0.06	<0.06	<0.06	<0.06
108.....	-14.82(38)	-13.694(12)	<0.16	<0.07	0.41(04)	0.32(04)
109.....	-9.6262(57)	-9.7838(29)	<0.06	<0.06	<0.06	<0.06
110.....	-14.21(15)	-13.812(20)	0.75(12)	0.34(05)	0.24(05)	0.57(05)
111.....	-11.7394(76)	-11.5679(28)	-0.08(03)	-0.11(03)	-0.11(03)	0.28(03)
113.....	-13.020(23)	-12.3902(51)	<0.07	<0.06	<0.06	<0.06
116.....	-12.3074(49)	-12.0825(20)	-0.29(03)	-0.34(03)	-0.36(03)	<0.06
117.....	-13.965(52)	-13.6496(81)	0.75(06)	0.42(04)	0.50(04)	0.92(04)
118.....	-11.3752(30)	-11.4750(26)	<0.06	<0.06	0.18(03)	0.20(03)
119.....	-13.305(36)	-13.0220(70)	0.08(04)	<0.06	<0.06	<0.06
120.....	-13.577(45)	-13.0193(69)	<0.08	<0.06	<0.06	0.15(03)
121.....	-11.8586(66)	-11.7800(40)	<0.06	<0.06	<0.06	<0.06
122.....	-14.305(76)	-13.771(17)	...	<0.07	<0.07	0.44(04)
125.....	-13.608(12)	-13.5367(51)	0.43(03)	0.32(03)	0.31(03)	0.19(03)
129.....	-10.9995(38)	-10.9344(27)	<0.06	<0.06	<0.06	0.15(03)
130.....	-12.763(11)	-12.7473(86)	<0.06	-0.08(03)	0.12(03)	0.28(04)
131.....	-10.657(17)	-10.639(15)	<0.07	<0.07	<0.07	<0.07
132.....	-14.38(11)	-13.0025(40)	...	-0.40(03):	-0.64(03):	0.33(03)
133.....	-11.531(12)	-11.0947(61)	<0.06	<0.06	<0.06	<0.06
134.....	-9.3389(100)	-9.667(11)	<0.06	<0.06	<0.07	<0.07
135.....	-13.179(11)	-12.9393(71)	0.54(03)	0.40(03)	0.45(03)	2.06(05)
137.....	-13.054(19)	-12.1374(28)	-0.37(03)	-0.41(03)	-0.26(03)	<0.06
138.....	-13.063(54)	-12.6083(74)	<0.08	<0.07	<0.06	<0.06
139.....	-12.375(13)	-11.7964(45)	<0.06	-0.07(03)	<0.06	0.08(03)
144.....	-12.278(34)	-11.9446(86)	<0.08	-0.14(03)	<0.06	0.28(03)
147.....	-11.657(32)	-11.4513(68)	<0.08	<0.07	<0.06	<0.06
150.....	-12.488(10)	-12.1919(31)	<0.06	<0.06	<0.06	<0.06

TABLE 9—Continued

ID (1)	log cnt2257 (2)	log cnt3060 (3)	Fe II 2379 Å (4)	Fe II 2600 Å (5)	Fe II 2742 Å (6)	Mg II 2798 Å (7)
154.....	-11.3323(94)	-11.2466(46)	-0.15(03)	-0.12(03)	-0.09(03)	<0.06
155.....	-11.001(10)	-11.0539(39)	0.07(03)	<0.06	<0.06	<0.06
156.....	-12.443(34)	-12.3456(87)	<0.07	<0.07	<0.07	<0.06
157.....	-11.476(12)	-11.1967(36)	-0.34(03)	-0.36(03)	-0.32(03)	0.80(04)
158.....	-12.564(43)	-12.541(12)	0.29(04)	0.37(04)	0.62(04)	0.50(03)
160.....	-13.606(71)	-12.8597(81)	0.10(04)	-0.10(03)	<0.06	<0.06
161.....	-13.69(15)	-12.5496(62)	0.18(06)	<0.07	<0.06	<0.06
162.....	-11.991(28)	-11.9714(83)	<0.07	<0.06	<0.06	<0.06
166.....	-11.404(20)	-11.3548(85)	<0.07	<0.07	<0.06	<0.06
171.....	-13.089(45)	-12.4578(64)	0.11(04)	<0.07	0.13(03)	<0.07
181.....	-12.374(36)	-11.9918(62)	<0.08	-0.12(03)	-0.09(03)	0.48(03)
184.....	-12.0982(54)	-11.6555(20)	<0.06	<0.06	<0.06	0.56(04)
196.....	-14.83(26)	-14.239(20)	<0.14	-0.09(03)	0.38(04)	0.30(04)
205.....	-13.27(10)	-12.510(10)	<0.10	-0.15(03)	-0.11(03)	0.18(03)
208.....	<-14.6	-13.557(17)	<0.45	<0.08	0.19(04)	0.16(04)
209.....	-13.68(23)	-12.3709(65)	0.14(06)	<0.07	<0.07	<0.06
210.....	-14.119(39)	-13.6931(64)	1.67(05)	1.47(04)	2.02(06)	1.40(05)
211.....	<-15.1	-13.6663(97)	<0.65	-0.08(04)	<0.07	<0.07
213.....	-12.910(18)	-12.6877(53)	<0.07	<0.06	<0.06	<0.06
214.....	-14.61(36)	-13.326(17)	<0.78	-0.22(05)	<0.08	<0.08
215.....	-11.4592(56)	-11.2829(29)	-0.16(03)	-0.19(03)	-0.20(03)	0.33(03)
218.....	-14.35(21)	-12.7991(45)
221.....	-12.818(11)	-12.5319(45)	0.07(03)	<0.06	<0.06	<0.06
222.....	-14.46(27)	-13.553(12)	...	-0.12(04)	-0.17(04)	0.53(04)
224.....	-11.660(18)	-11.5379(66)	<0.06	<0.06	<0.06	<0.06
225.....	-13.642(22)	-13.1294(34)	-0.12(03)	-0.13(03)	<0.06	0.58(03)
226.....	-11.8929(57)	-11.6723(40)	-0.19(03)	-0.28(03)	-0.19(03)	0.17(03)
227.....	-14.16(22)	-13.004(18)	<0.13	<0.07	<0.08	<0.08
231.....	-11.588(12)	-11.3573(45)	<0.06	<0.06	<0.06	<0.06
232.....	-13.055(44)	-12.502(15)	<0.08	-0.07(03)	<0.07	<0.07
233.....	-14.621(99)	-13.9991(75)	<0.11	<0.07	<0.07	0.11(03)
234.....	-13.669(99)	-12.915(21)	-0.25(05)	-0.19(04)	<0.08	0.51(06)
237.....	<-15.1	-13.8281(84)	...	-0.46(05)	-0.41(04)	<0.07

NOTES.—Continuum spectral fluxes are in units of $\text{ergs s}^{-1} \text{cm}^{-2} \text{\AA}^{-1}$. Excess line emission is unitless. Uncertainties in the last two digits are enclosed in parentheses after each value. Tabulated upper limits are twice the measured uncertainty. The absence of data in an entry implies that line excess could not be measured, due to a poor template fit. Table 9 is also available in machine-readable form in the electronic edition of the *Astrophysical Journal Supplement*.

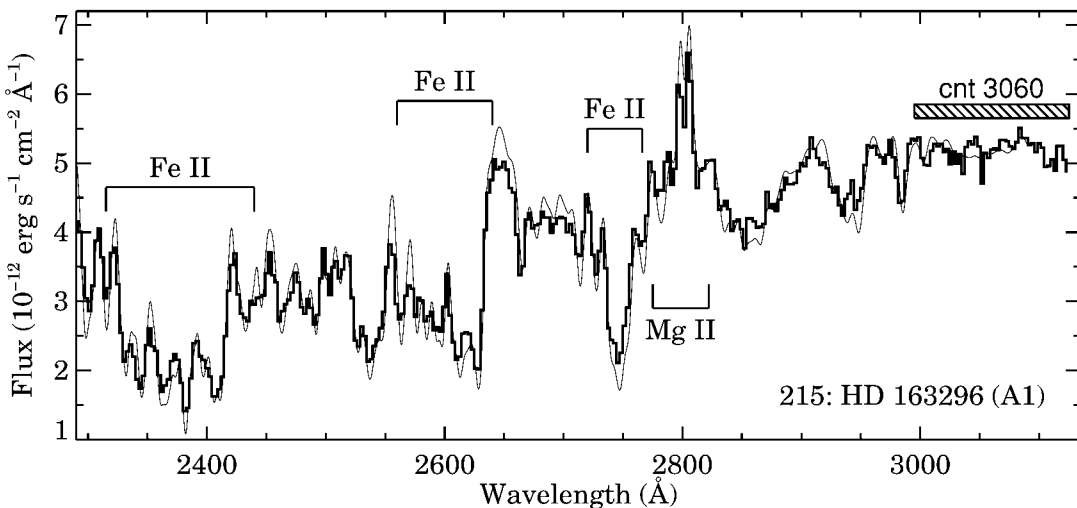


FIG. 8.—Combined IUE LW spectrum (dark histogram) of the HAEBE star HD 163296 with wavelength intervals of interest marked and identified. The superposed STIS spectrum (light curve) matches well after being degraded to a resolution of 6 Å.

TABLE 10
NUMBER OF STARS WITH NUV SPECTRA

Category (1)	GHRS	STIS	<i>HST</i>		<i>IUE</i>
	Only (2)	Only (3)	Both (4)	Total (5)	LW (6)
HAEBE.....	1	5	0	6	97
CTTS.....	0	11	8	19	77
NTTS.....	2	1	0	3	29
FU Ori.....	0	1	0	1	1
Total.....	3	18	8	29	204

4.1. Variability

Figure 9 shows fractional variability amplitudes, A , and upper limits from Table 3 as a function of spectral class. As in Figure 2 of Paper I, TTS variability amplitude increases toward the latest spectral classes, presumably because at *IUE* wavelengths hot emission due to accretion or activity dominates progressively cooler photospheric emission. NTTS can vary significantly due to magnetic activity, as demonstrated by V410 Tau (no. 10), V987 Tau (no. 16), and NV Ori (no. 96). In the SW data alone (Paper I) the apparent decrease in variability toward F and early-G spectral classes was ambiguous because of the paucity of such stars. Spectral class F stars are also rare in the LW sample, but four out of the five with multiple *IUE* observations show typical variability, so variability mechanisms apparently operate equally well for F stars. HAEBE stars show more than 10% variability in 41% of the LW sample, which equals the 41% rate in the SW sample. These variability rates are subject to observational biases inherent in the *IUE* archive. The LW HAEBE data show no trend in variability amplitude with spectral type, despite hints of such a trend in the SW data.

The set of HAEBE stars with multiple *IUE* observations is too biased to draw firm statistical inferences about the incidence of UV variability, but our analysis does show that HAEBE stars of any spectral type can vary significantly. Finkenzeller & Mundt (1984) show that the incidence of V -band variability decreases dramatically for HAEBE stars with spectral class earlier than A0. Their variability threshold of 0.05 mag is comparable to our 5% threshold for detecting changes in A , though the typical amplitude of variations may be different at visual and UV wavelengths. Similarly, Herbst & Shevchenko (1999) find V -band variability greater than 0.2 mag in 15 out of 41 HAEBE stars with spectral classes later than B7, but they find no such variability in 19 earlier type HAEBE stars. Evidently, variability in early-

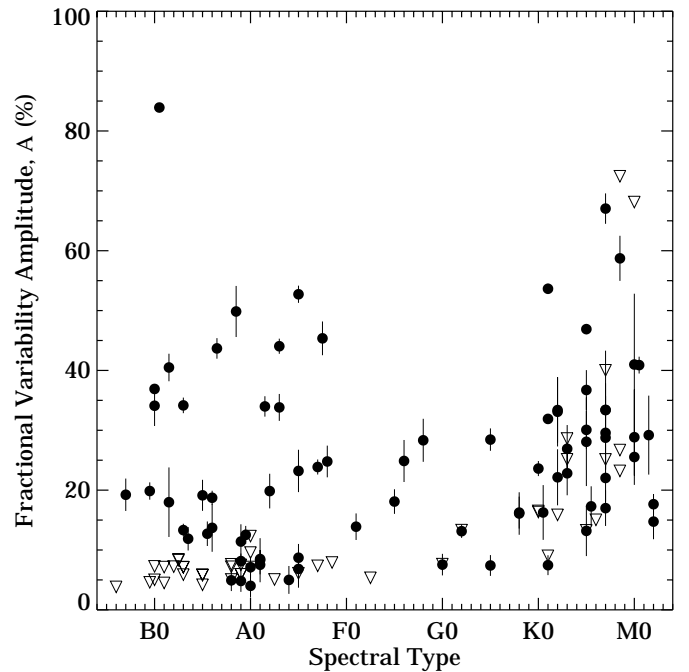


FIG. 9.—Mean deviation in 1900–3200 Å flux, relative to the global mean for all spectra of a given PMS star. Triangles indicate 2σ upper limits. Only stars observed more than once by *IUE* are shown. Few PMS stars of spectral class F were observed by *IUE*, but LW data are adequate to show that they can vary significantly.

type HAEBE stars is more prominent in the UV than in the visual.

Figure 10 statistically compares values of A as a function of bandpass for both TTS and HAEBE stars. Variability amplitudes come from Table 3 (LW) and Table 4 of Paper I (SW). We only consider sources with A greater than $2\sigma_A$ in both *IUE* bandpasses. We fitted a power law, jointly considering uncertainties in both axes, obtaining

$$\log A_{\text{SW}} = 0.248(58) + 0.794(37) \log A_{\text{LW}}, \quad (2)$$

where parentheses enclose the formal uncertainty in the two least significant digits of each coefficient. A χ^2_{ν} of 12.6 implies significant scatter about the fitted power law, due in part to different temporal sampling in the SW and LW bandpasses. Given the observed scatter about the fitted power law, there is no statistically significant difference between the fitted power law and a model in which variations have equal amplitude in both *IUE* bandpasses. Fitting TTS and HAEBE stars separately yields a similar result.

The statistical similarity between SW and LW variability amplitudes in Figure 10 can be explained by a variety of models. For example, small changes in A_V give rise to similar variability amplitudes in both *IUE* bandpasses, independent of spectral shape or the mean value of A_V . Figure 10 shows the predicted variability amplitudes for uniform A_V variations with a full range of 0.05–0.25 mag. The SW extinction variations are only 15% larger than the LW variations due to strong localized absorption near 2200 Å. Similarly, changes in accretion rate or activity level yield equal variability amplitudes in both *IUE* bandpasses, if the spectral shape of the variable component does not change with brightness and if the constant component is either negligible or has a spectrum that is similar to the variable component.

TABLE 11
NUMBER OF STARS WITH FUV SPECTRA

Category (1)	GHRS	STIS	<i>HST</i>		<i>IUE</i>
	Only (2)	Only (3)	Both (4)	Total (5)	SW (6)
HAEBE.....	0	5	2	7	71
CTTS.....	2	8	7	17	38
NTTS.....	4	2	0	6	8
FU Ori.....	0	0	0	0	1
Total.....	6	15	9	30	118

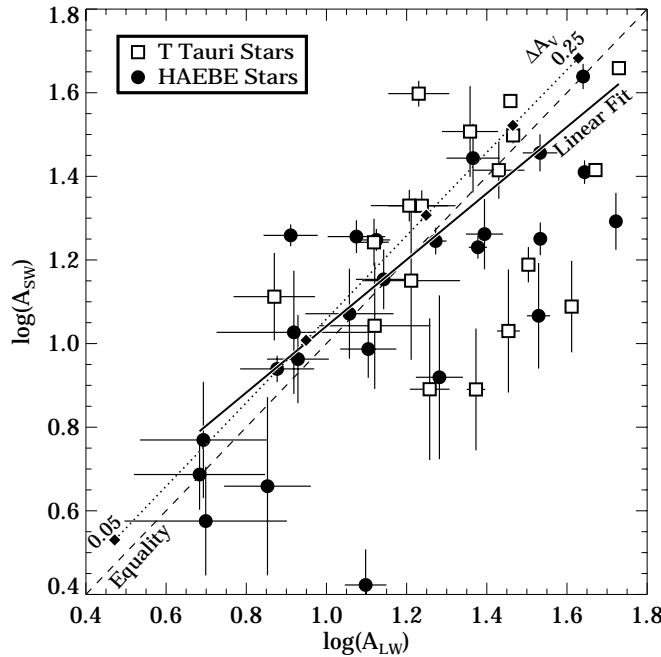


FIG. 10.—Comparison of logarithmic variability amplitudes for TTS (squares) and HAEBE stars (circles) in *IUE* long- and short-wavelength bandpasses. Formal errors smaller than the plot symbol are not shown. The solid line shows a linear fit, which corresponds to a power-law relationship between variability amplitudes. A dashed line shows the locus of equal amplitude variations in both bandpasses. The dotted line shows the effect of extinction variations, with diamonds illustrating A_V variations of 0.05–0.25 mag.

For example, CTTS flux variations may be dominated by changes in the spatial extent of accretion footpoints, rather than density or temperature changes in these regions. This possibility is supported by observational evidence that CTTS with higher accretion rates tend to have larger filling factors (Valenti, Basri, & Johns 1993; Calvet & Gullbring 1998). Detailed studies of variability in individual stars are needed to definitively test various models.

4.2. UV Diagnostics of TTS Activity and Accretion

CTTS are distinguished from NTTS primarily by excess emission associated directly or indirectly with accretion of circumstellar disk material. In Paper II we used SW spectra of four warm NTTS to estimate for all TTS the C IV surface flux due to saturated magnetic activity. We then attributed any significant C IV excess in CTTS to emission produced by accretion shocks at the stellar surface. We found a good correlation between excess C IV emission and \dot{M} from Hartigan, Edwards, & Ghadour (1995) for 13 CTTS, leading to our claim that much of the *IUE* SW emission comes from accretion processes. The correlation was improved by using distances and stellar radii to convert excess surface flux into excess line luminosity. We determined an empirical relationship between \dot{M} and excess C IV line luminosity and that allowed us to estimate \dot{M} for 15 additional CTTS with no previous measurements (see Table 4 of Paper II). A comparable analysis of Mg II emission would be quite interesting, so we begin here by describing observational characteristics of the *IUE* sample.

The Mg II doublet near 2800 Å is the most prominent emission feature in LW spectra of TTS. Although Mg II

forms at cooler temperatures than C IV, many more TTS have Mg II measurements, so it is useful to explore the diagnostic potential of Mg II. Columns (1) and (2) of Table 12 list the identification number and TTS category from Table 1 for most TTS with an observed “Mg II 2798 Å” line flux in Table 6. Only four isolated TTS are excluded for lack of credible distance estimates, namely LkH α 333 (No. 55), HD 288313 (No. 115), V4046 Sgr (No. 216), and BP Psc (No. 238). Column (3) of Table 12 gives the logarithm of intrinsic line luminosity (L_{Mg}), which equals the observed line flux times $4\pi d^2$ and $6.0A_V$, where the latter factor removes the effects of extinction at 2800 Å. The final columns of the table give distance (d) and A_V used in the calculation of L_{Mg} , each followed by literature reference codes defined in the table notes.

Figure 11 shows the relationship between our measured “Mg II 2798 Å” line fluxes in Table 6 and literature values of A_V in Table 12. For TTS in the *IUE* sample, there is no significant correlation between observed Mg II flux and A_V , even though observed line fluxes are diminished by extinction factors of 1 to 200 from left to right across Figure 11. Correcting observed fluxes for differences in distance still leaves a threshold below which no TTS are detected. In principle increasing intrinsic line luminosity could exactly compensate for increasing extinction at 2800 Å, but more likely the lower envelope in Figure 11 indicates the practical detection limit for *IUE*. The existence of this detection limit introduces a bias in the sample of stars with useful *IUE* data, such that minimum intrinsic line luminosity must increase with A_V . We adopt the lowest measured Mg II flux ($3.0 \times 10^{-14} \text{ erg s}^{-1} \text{ cm}^{-2}$ for the NTTS V1074 Tau, No. 24) as the practical limit below which *IUE* could not detect Mg II emission. Co-added spectra have a range of noise levels, so use of a unique detection limit is only an approximation.

Figure 12 plots $\log L_{\text{Mg}}$ from column (3) of Table 12 versus A_V from column (4). TTS line luminosities span four orders of magnitude. There is a strong correlation between L_{Mg} and A_V , due at least in part to the observational bias that was demonstrated in Figure 11. Diagonal dashed lines in Figure 12 show our adopted *IUE* detection limit translated to the mean distances of the Taurus-Auriga and Orion star forming regions. At low extinction where observational bias is less of an issue, NTTS typically have lower intrinsic line luminosities than CTTS. This behavior is consistent with the hypothesis that L_{Mg} and UV flux in general scales with \dot{M} , but more detailed analysis is needed. In particular, stellar radii should be used to assess and remove the contribution from magnetic activity, yielding excess L_{Mg} . Given the results of Paper II and preliminary LW tests, excess L_{Mg} is probably correlated with \dot{M} , suggesting that accretion related processes may contribute significantly to the LW emission from CTTS. However, excess L_{Mg} is also correlated with A_V because of the sample bias discussed above, complicating the interpretation if circumstellar extinction is higher around CTTS with higher mass accretion rates.

Certain outliers in Figure 12 are worthy of specific mention. IK Lup (M0, No. 163) and GW Lup (M2, No. 165) are significantly less luminous than other CTTS. Barring an error in A_V or distance, these two CTTS demonstrate that accretion need not generate high line luminosity, especially at late spectral types where low accretion rates are more easily detected. Extended nebular emission (Panek 1983), rather than accretion, may elevate line luminosity for five NTTS with $L_{\text{Mg}} \sim 10^{31} \text{ ergs s}^{-1}$. A similar caveat may apply

TABLE 12
INTRINSIC Mg II LINE LUMINOSITY

ID	TTS Cat. ^a	$\log L_{\text{Mg}}$ (ergs s ⁻¹)	A_V	Ref.	d (pc)	d Ref.
(1)	(2)	(3)	(4)	(5)	(6)	(7)
3.....	C	31.8	0.85	L01	275	L01
7.....	N	30.8	1.32	K95	140	H95
8.....	C	29.6	0.26	W01	140	H95
9.....	C	31.6	2.21	W01	140	H95
10.....	N	29.9	0.00	S89	140	H95
11.....	N	29.4	0.00	Avg ^b	140	H95
12.....	C	30.9	0.51	G98	140	H95
13.....	N	29.9	1.23	Avg ^b	140	H95
14.....	C	30.8	0.62	G98	140	H95
15.....	C	31.0	0.29	J00	140	H95
16.....	N	30.2	0.49	Avg ^b	140	H95
17.....	C	31.8	1.00	B88	140	H95
18.....	C	30.4	0.45	G98	140	H95
19.....	C	31.7	1.66	J00	140	H95
20.....	N	29.6	0.05	Avg ^b	140	H95
21.....	N	29.9	1.08	S89	140	H95
22.....	N	29.5	0.26	W01	140	B99
23.....	C	30.9	1.42	G98	140	H95
24.....	N	29.0	0.18	Avg ^b	140	H95
26.....	N	29.1	0.00	Avg ^b	140	H95
27.....	N	29.6	0.46	Avg ^b	140	H95
29.....	C	30.9	0.60	G98	140	H95
31.....	C	30.9	1.00	W01	140	H95
33.....	C	30.2	0.36	W01	140	H95
34.....	N	29.6	0.41	Avg ^b	140	H95
35.....	C	30.5	1.34	G98	140	H95
36.....	C	30.3	0.94	G98	140	H95
37.....	C	30.5	0.88	J00	140	H95
40.....	C	30.1	0.74	G98	140	H95
41.....	C	29.9	0.25	G98	140	H95
44.....	C	30.4	0.71	G98	140	H95
45.....	C	31.0	2.18	C79	140	H95
46.....	C	31.5	1.66	J00	140	H95
47.....	C	30.4	0.34	G98	140	H95
48.....	C	31.2	1.26	G98	140	H95
49.....	C	30.3	0.31	G98	140	H95
50.....	N	29.5	0.00	W88	140	H95
52.....	C	31.1	0.93	B88	140	H95
56.....	C	32.3	1.14	J00	140	H95
59.....	C	33.1	2.20	E02	460	C79
61.....	C	32.3	0.82	B90	460	C79
62.....	C	31.5	0.27	C79	460	C79
64.....	N	29.3	0.00 ^c	...	14	E97
66.....	C	31.6	1.30	E02	460	C79
67.....	N	31.2	0.00	C00	500	S91
68.....	C	31.7	0.36	C79	460	C79
69.....	C	31.6	0.57	G95	460	C79
81.....	N	31.2	0.32	C79	460	C79
96.....	N	31.3	0.50	L68	460	C79 ^d
97.....	C	31.4	0.97	C79	460	C79
102.....	N	31.0	0.20	S90	460	C79 ^d
104.....	C	31.3	0.00	C79	460	C79
105.....	N	30.9	0.36	S90	460	C79 ^d
112.....	C	31.3	0.28	C79	460	C79
114.....	F	33.4	2.50	L88	480	L88
124.....	N	<30.9	0.00	C79	800	C79
126.....	C	<30.7	0.13	F91	700	F91
140.....	C	29.9	0.21	G92	170	B99
141.....	C	32.3	2.99	G92	170	B99
142.....	C	30.8	1.37	G92	170	B99
143.....	C	30.1	0.00	M00	56	E97
145.....	C	30.7	0.85	G92	170	B99
146.....	C	30.3	0.14	G92	170	B99

TABLE 12—Continued

ID	TTS Cat. ^a	$\log L_{\text{Mg}}$ (ergs s ⁻¹)	A_V	Ref.	d (pc)	d Ref.
(1)	(2)	(3)	(4)	(5)	(6)	(7)
148.....	C	31.5	2.35	G92	170	B99
149.....	C	31.8	2.39	G92	170	B99
151.....	C	29.9	0.47	G92	170	B99
152.....	C	30.8	1.17	G92	170	B99
153.....	C	32.2	1.67	G92	170	B99
163.....	C	29.3	0.20	H94	140	G92
164.....	C	31.2	1.45	H94	140	G92
165.....	C	29.3	0.00	H94	140	G92
167.....	C	30.2	0.79	H94	140	G92
168.....	N	<29.8	0.20	W94	160	W94
169.....	C	29.9	0.98	H94	140	G92
170.....	C	32.1	1.28	H94	140	H94
172.....	C	30.5	0.55	H94	140	G92
174.....	C	29.9	0.37	H94	140	G92
175.....	C	30.1	0.65	B90	140	H94
176.....	N	29.6	0.20	W94	160	W94
177.....	N	29.7	0.20	W94	160	W94
178.....	C	29.9	0.00	H94	140	H94
180.....	C	30.8	1.25	H94	140	H94
182.....	C	29.7	0.50	H94	140	G92
183.....	C	30.7	0.82	H94	140	H94
188.....	C	31.8	2.23	V93	160	L96
189.....	N	<29.9	1.40	W94	160	W94
190.....	N	30.7	1.30	W94	160	W94
191.....	N	<29.3	0.60	W94	160	W94
192.....	C	31.3	1.70	H92	160	H92
194.....	C	31.4	1.84	B90	170	C79
199.....	C	30.6	0.50	B90	170	C79
200.....	C	29.9	0.14	C79	170	C79
201.....	C	30.0	0.00	C79	170	C79
202.....	C	30.9	1.16	C79	170	C79
204.....	N	<30.2	2.10	W94	160	W94
206.....	C	31.6	1.15	V93	160	H92
207.....	C	31.1	0.40	A89	145	D99
217.....	C	30.5	0.31	H86	106	E97
219.....	C	30.2	0.50	H92	130	H92
220.....	N	29.8	0.84	W86	130	H92
230.....	C	32.5	1.30	H92	700	H92
236.....	C	31.6	0.90	H92	300	H92

^a TTS category codes: (C) CTTS, (N) NTTS, and (F) FU Ori.^b Tabulated A_V is the mean of values in Cohen & Kuhi 1979 and Strom et al. 1990.^c Assumed $A_V = 0$ due to proximity of star.^d Distance assumed by analogy to Cohen & Kuhi 1979 distance for other Orion TTS.

REFERENCES.—(A89) Andersen et al. 1989; (B88) Bertout et al. 1988; (B90) Bouvier 1990; (B99) Bertout et al. 1999; (C79) Cohen & Kuhi 1979; (C00) Chavarría-K et al. 2000; (D99) de Zeeuw et al. 1999; (E97) ESA 1997; (E02) Eiroa et al. 2002; (F91) Feldbrugge & van Genderen 1991; (G92) Gauvin & Strom 1992; (G95) Gagné et al. 1995; (G98) Gullbring et al. 1998; (H86) Herbig & Goodrich 1986; (H92) Hamann & Persson 1992; (H94) Hughes et al. 1994; (H95) Hartigan et al. 1995; (J00) Paper II; (K95) Kenyon & Hartmann 1995; (L68) Lee 1968; (L88) Levreault 1988; (L96) Liu et al. 1996; (L01) Luhman 2001; (M00) Muzerolle et al. 2000; (S89) Strom et al. 1989; (S90) Strom et al. 1990; (S91) Skinner et al. 1991; (V93) Valenti et al. 1993; (W86) Walter 1986; (W88) Walter et al. 1988; (W94) Walter et al. 1994; (W01) White & Ghez 2001.

to large aperture observations of other TTS in Orion. Line luminosity may also be enhanced in magnetically active stars with relatively large radii or in systems with multiple components. The PMS stars with the largest L_{Mg} are FU Ori (No. 114) and then CO Ori (No. 59). Extremely large mass accretion rates have been inferred for FU Ori

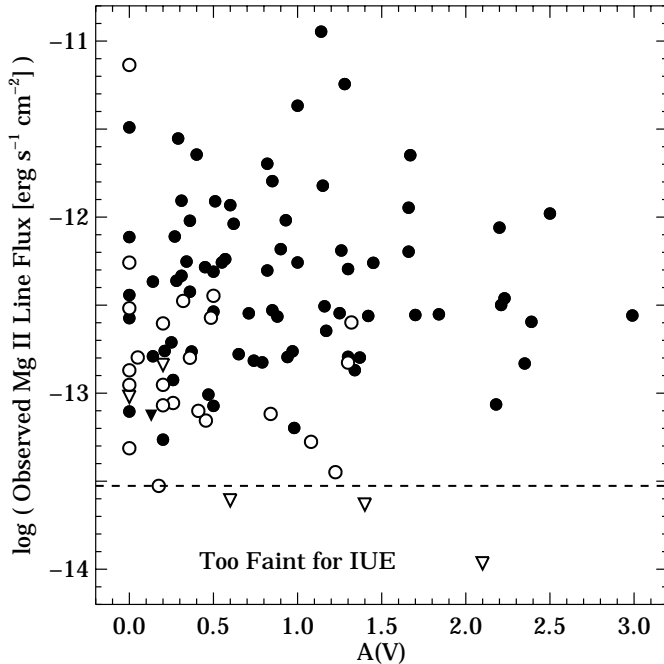


FIG. 11.—Logarithm of observed “Mg II 2798 Å” line flux (Table 6) vs. visual extinction from the literature (Table 12). Plot symbol types distinguish detections (*circles*) from 2σ upper limits (*triangles*) and CTTS (*filled*) from NTTS (*unfilled*). The horizontal dashed line at 3.0×10^{-14} erg s^{-1} cm^{-2} indicates the approximate flux limit below which Mg II was not detected by *IUE*.

(Kenyon, Hartmann, & Hewett 1988). V1074 Tau (No. 24) has the smallest L_{Mg} at 1.0×10^{29} ergs s^{-1} . Note that in Figure 11, the zero-age main-sequence star AB Dor (No. 64), has the second largest observed flux because it is nearby (14 pc), not because it is intrinsically luminous.

Blueshifted absorption components in high-resolution Mg II profiles indicate that outflow optical depths can be significant in some CTTS (e.g., Imhoff & Appenzeller 1987; Ardila et al. 2002). Thus, outflows may also contribute significantly to Mg II emission, as in spherical wind models by Hartmann et al. (1990). High-resolution line profiles of Mg II and Fe II would help constrain wind models, as in evolved stars (e.g., Carpenter et al. 1999), but CTTS models must also include accretion flows and shocks, as in existing analyses of Balmer line profiles (e.g., Hartmann, Hewett, & Calvet 1994; Muzerolle, Calvet, & Hartmann 1998, 2001). For our purposes here, we loosely refer to accretion and outflows as “accretion related processes,” since they are linked observationally (e.g., Cabrit et al. 1990; Valenti et al. 1993; Hartigan et al. 1995) and theoretically (e.g., Shu et al. 1994).

4.3. Herbig Ae/Be Stars

HAEBE stars are well defined from an evolutionary standpoint, but observational signatures are imprecisely defined. The presence of emission or anomalous absorption lines indicates peculiarity, but youth is not the only explanation. In particular, normal Be stars may also show emission due to accretion from a companion, and various types of outflows (e.g., planetary nebulae, Wolf-Rayet stars) give rise to circumstellar absorption. Herbig (1960) defines HAEBE stars as early-type stars with emission lines, in obscured regions, and illuminating nearby nebulosity. Thé et al. (1994) discuss a much broader range of potentially dis-

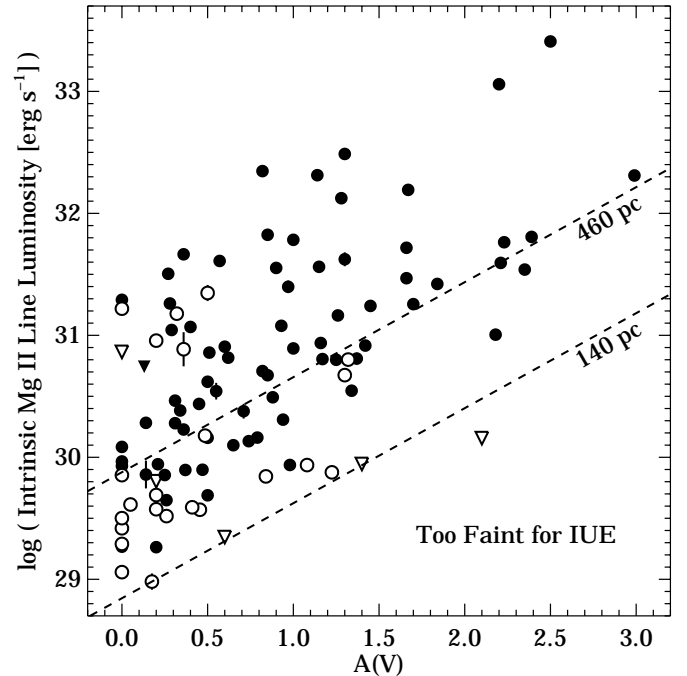


FIG. 12.—Similar to Fig. 11, except the ordinate is the logarithm of intrinsic Mg II line luminosity, calculated from “Mg II 2798 Å” line flux using values of distance and extinction in Table 12. Diagonal dashed lines map the *IUE* detection limit in Fig. 11 to distances of 140 and 460 pc. The paucity of high- A_V , low-luminosity sources below the diagonal lines is an observational bias.

tinctive observational characteristics. With the low-resolution UV spectra compiled here and in Paper I, it is appropriate to investigate the UV characteristics of HAEBE stars, which may in some cases distinguish HAEBE stars from other classes of unusual objects.

Figure 2 shows that UV spectra of HAEBE stars generally consist of a reddened continuum that is characteristic of the adopted spectral type, as expected. Narrow absorption features are weak or absent in roughly half the *IUE* spectra, especially for hotter HAEBE stars, not unlike *IUE* spectra of main-sequence extinction templates shown in Figure 6. For later spectral types, the *absence* of absorption features may be an indication of spectral peculiarity. For example, Figure 2 shows Mg II 2800 Å in absorption for V351 Ori (A7, No. 113), yet Table 9 indicates no anomalous emission or absorption. In contrast, Mg II is not apparent in V856 Sco (A7, No. 184), yet Table 9 indicates a highly significant excess. These results follow from the strong Mg II absorption present in the A7 template spectrum shown in Figure 6. An apparent excess in line emission can be due to line emission or to significant continuum veiling.

A significant fraction of the candidate HAEBE stars in the *IUE* sample show no evidence of their youthful nature in moderately noisy NUV spectra at low resolution. Our candidate HAEBE stars are drawn mainly from the catalog of Thé et al. (1994), which uses IR excess as a key selection criterion. Some candidates may ultimately prove to be older stars that are misclassified as HAEBE stars, but it is tempting to identify candidate HAEBE stars with ordinary UV spectra as higher mass analogs of NTTS. If the analogy is valid, then HAEBE stars with peculiar UV spectra would be accreting analogs of classical TTS, while those with normal UV spectra would be nonaccreting analogs of NTTS. To

begin exploring this hypothesis, we now discuss the occurrence of various spectral anomalies in LW *IUE* spectra of HAEBe stars.

Table 9 indicates that 55 out of 97 HAEBE stars have significant excess absorption or emission in at least one of the Fe II windows centered at 2379, 2600, and 2742 Å. In 23 stars, all three windows are either significantly in absorption (12 stars) or emission (11 stars). All the HAEBE stars with Fe II consistently in absorption are spectral class A4 or earlier. Their mean spectral class is A0 with a standard deviation of 3 spectral subclasses. With the exception of V590 Mon (B8, No. 125) and He 3-847 (B5, No. 158), all the HAEBE stars with Fe II consistently in emission are spectral type A0 or later. The mean spectral class of these nine stars is A6 with a standard deviation of 3 spectral subclasses. Thus, HAEBE stars with prominent NUV lines of Fe II are typically in absorption for spectral classes A3 and earlier and in emission for later spectral classes. The corresponding stellar effective temperature at this spectral class boundary is about 8300 K, suggesting this as a rough formation temperature for the Fe II features, assuming substantial optical depth and geometrical extent equivalent to the photosphere.

In contrast to the spectral type dependence of Fe II excess absorption or emission, Mg II rarely exhibits excess absorption. Excess Mg II emission is significant in 47 out of 97 HAEBE stars, but only LP Ori (B1.5, No. 80), LZ Ori (A0, No. 87), and V346 Ori (A5, No. 58), exhibit marginally significant excess absorption in Mg II. The origin of this excess absorption is not understood. Interstellar line absorption should not be significant because extinction toward these three stars is relatively low (see Table 8), and wind absorption is also unlikely because no other lines appear in the spectra. A different set of HAEBE stars have excess Fe II absorption, indicating the presence of a wind, but apparently normal Mg II in Table 9. Many of these stars have P Cygni profiles, even at *IUE* resolution (about 640 km s^{-1}). The most obvious examples are He 3-1428 (B0, No. 213), MWC 1080 (B0, No. 237), HD 87643 (B3.5, No. 137), HD 250550 (B9, No. 116), AB Aur (B9.5, No. 51), and HD 179218 (B9.5, No. 224). For these stars, emission and absorption largely cancel in our adopted Mg II wavelength interval (see Table 5). In *IUE* spectra of a few other HAEBE stars, emission and blueshifted absorption components are both present in unequal proportions. Figure 13 plots excess Mg II emission from Table 9 as a function of spectral class. Excess emission increases toward later spectral types, perhaps indicating increasing contrast of an accretion or outflow component.

Hillenbrand et al. (1992) used IR photometry to separate HAEBE stars into three classes (I, II, and III) associated with different circumstellar environments. *IUE* observed 26 of 30 class I sources with IR excesses characteristic of an accretion disk. Excluding VV Ser (A0, No. 218) for which our template fitting procedure failed, 21 of 25 class I sources have peculiar UV spectra with at least one anomalous line strength. Exceptions such as CU Cha (A0, No. 150) have normal UV spectra despite an IR excess indicative of a disk. Class II sources have IR characteristics suggesting emission from an envelope and possibly a disk. Three of four class II sources with useful *IUE* spectra have anomalous UV line strengths. Class III sources are usually associated with NTTS because normal IR colors rule out the presence of a disk. All three class III stars with useful *IUE* spectra have normal UV spectra. While there are exceptions, the presence

or absence of UV spectral peculiarities correlates well with IR classifications from Hillenbrand et al. (1992), connecting UV accretion and wind diagnostics with IR signatures of infalling material.

Corcoran & Ray (1997) separate HAEBE stars into categories (I, IIa, IIb, III, and IV) that define a sequence of progressively lower blueshifts of the [O I] emission line near 6300 Å. Category I and IIa sources have large or moderate blueshifts associated with jets (Hartigan et al. 1995). Category IIb sources have small blueshifts, but no supporting optical or radio evidence of outflows. Category III and IV sources have zero velocity or moderate redshifts with no evidence of outflows. Proceeding in sequence, there are one, five, three, zero, and five HAEBE stars with useful *IUE* spectra in each category. Following the same sequence, one, four, one, zero, and three of the stars have peculiar UV spectra. Although the statistics are poor, it seems that UV peculiarity is not well correlated with [O I] signatures of jets and outflows. If we accept that UV peculiarity typically implies accretion and/or outflows, then the velocity shift of [O I] may not be a robust indicator of these processes.

Accretion shocks at the surface of a CTTS produce observable veiling and excess blue emission because gas is heated to 10^4 K, which is significantly hotter than the photosphere. Veiling has not been detected in high-resolution optical spectra of HAEBE stars, perhaps because the photosphere and shocked gas have similar temperatures (Ghandour et al. 1994). Contrast might be improved in the UV, so we investigated the effect of a hypothetical veiling continuum on LW spectral shape and line strength. As a simple numerical experiment, we constructed veiled HAEBE spectra by combining main-sequence template spectra in Figure 6 with a 10^4 K blackbody assumed to cover 5% of the stellar surface. We fitted each artificial spectrum of a HAEBE star with the original template spectra,

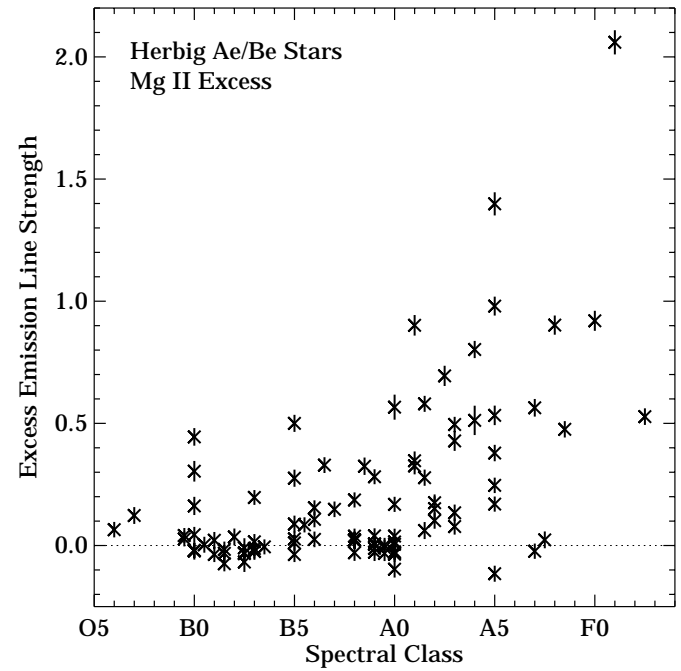


FIG. 13.—Excess Mg II line emission in HAEBe stars, relative to mean line depths in main-sequence templates of the same spectral class. Excess emission increases toward later spectral types, perhaps indicating increasing contrast of an accretion or outflow component.

redetermining A_V and apparent spectral class. Errors in apparent spectral class decreased from about 1 subclass at F0 to a few tenths of a subclass at A0, while errors in A_V decreased from 0.05 to 0.01 magnitude over the same spectral class range. These small errors cannot be measured reliably in *IUE* spectra. On the other hand, veiling is strong at spectral class F0 and is still detectable at spectral class A5, appearing as excess line emission relative to main-sequence templates (see § 3.5). Thus, excess line emission in HAEBE stars later than spectral class A0 could be due to veiling. For spectral classes earlier than A0, addition of a 10^4 K blackbody has no significant effect on the composite spectrum because the hot photospheric spectrum is dominant.

C. M. J.-K. acknowledges partial support from NASA grant NAG5-8209. All of the data presented in this paper were obtained from the Multi-Mission Archive at the Space Telescope Science Institute (MAST). STScI is operated by the Association of Universities for Research in Astronomy, Inc., under NASA contract NAS5-26555. Support for MAST for non-*HST* data is provided by the NASA Office of Space Science via grant NAG5-7584 and by other grants and contracts. This research made use of the NASA Astrophysics Data System Bibliographic Services. This research made use of the SIMBAD database, operated at CDS, Strasbourg, France.

APPENDIX

Section 2.2 describes the procedure we used to assess individual spectra, prior to constructing a combined spectrum for each source. During this procedure, we made note of the spectral characteristics listed in Tables A1 and A2. These two tables also define corresponding status codes, which are used in Table A3 to indicate which of the spectra we considered have these characteristics.

TABLE A1
STATUS CODES FOR INCLUDED SPECTRA

Code (1)	Meaning (2)
0.....	No comment
1.....	Fails one or more quality tests
2.....	Relatively noisy spectrum
3.....	Questionable spectral feature near 3150 Å
4.....	Spectrum is anomalously strong
5.....	Questionable spectral feature near 3075 Å
6.....	Questionable spectral feature near 2900 Å
7.....	Questionable spectral feature near 2500 Å
8.....	Spectrum is anomalously weak
9.....	Relatively noisy small aperture spectrum
10.....	Questionable small aperture spectral feature near 2875 Å
11.....	Questionable small aperture spectral feature near 3200 Å
12.....	Many spectrum points flagged as bad
13.....	Questionable spectral feature near 3200 Å
14.....	Noisy spectrum
15.....	Negative excursions in flux near 3200 Å
16.....	Questionable spectral feature near 2350 Å
17.....	Mg II only
18.....	Questionable spectral feature near 2600 Å
19.....	Large aperture spectrum fails one or more quality tests
20.....	Questionable spectral feature near 3175 Å
21.....	Questionable spectral feature after 3050 Å
22.....	Questionable large aperture spectral feature near 2250 Å
23.....	Many small aperture spectrum points flagged as bad
24.....	Questionable spectral feature near 3100 Å
25.....	Relatively noisy large aperture spectrum
26.....	Questionable spectral feature near 2950 Å
27.....	Many large aperture spectrum points flagged as bad

TABLE A2
STATUS CODES FOR EXCLUDED SPECTRA

Code (1)	Meaning (2)
-1.....	Many spectrum points flagged as bad
-2.....	Probably not a PMS star
-3.....	No significant signal
-4.....	Very noisy spectrum
-5.....	Very noisy small aperture spectrum
-6.....	Fails one or more quality tests
-7.....	Spectrum is anomalously weak
-8.....	Very noisy large aperture spectrum
-9.....	Many large aperture spectrum points flagged as bad
-10.....	Large aperture spectrum fails one or more quality tests
-11.....	Many small aperture spectrum points flagged as bad
-12.....	Relatively noisy large aperture spectrum
-13.....	Different source in small aperture
-14.....	Different source in large aperture
-15.....	Scattered light
-16.....	Not available in final archive
-17.....	Excessive contamination from nearby hot stars
-18.....	Large aperture spectrum is anomalously weak
-19.....	Small aperture spectrum is anomalously weak
-20.....	Questionable spectral features in 2200–2600 Å range
-21.....	Small aperture spectrum has no significant signal
-22.....	Unusual continuum shape
-23.....	Spectrum is anomalously strong
-24.....	Relatively noisy small aperture spectrum
-25.....	Small aperture spectrum fails one or more quality tests
-26.....	Spectrum not used in sum
-27.....	Planetary nebula

TABLE A3
IUE OBSERVATIONS OF PMS STARS

ID ^a (1)	Sequence Number (2)	Status Code ^b (3)	Status Code ^b (4)
1.....	lwp29701	0	0
2.....	lwr02497	-1	0
2.....	lwr08062	0	0
2.....	lwr08063	0	0
2.....	lwr02496	0	0
3.....	lwp10051	0	0
3.....	lwp16942	0	0
3.....	lwp16943	0	0
4.....	lwp19651	-2	0
5.....	lwp05147	-3	0
6.....	lwp31507	0	0
7.....	lwp23901	0	0
7.....	lwp23902	0	0
7.....	lwp23903	-3	0
7.....	lwp23904	0	0
7.....	lwp23905	0	0
7.....	lwp02069	-4	0

NOTES.— Table A3 is available in its entirety in the electronic edition of the *Astrophysical Journal Supplement*. A portion is shown here for guidance regarding its form and content.

^a Identification number from col. (1) of Table 1.

^b Status codes are defined in Tables A1 and A2.

REFERENCES

- Andersen, J., Lindgren, H., Hazen, M. L., & Mayor, M. 1989, A&A, 219, 142
- Appenzeller, I., Krautter, J., & Jankovics, I. 1983, A&AS, 53, 291
- Ardila, D. R., & Basri, G. 2000, ApJ, 539, 834
- Ardila, D. R., Basri, G., Walter, F. M., Valenti, J. A., & Johns-Krull, C. M. 2002, ApJ, 567, 1013
- Basri, G., & Batalha, C. 1990, ApJ, 363, 654
- Bertout, C. 1989, ARA&A, 27, 351
- Bertout, C., Basri, G., & Bouvier, J. 1988, ApJ, 330, 350
- Bertout, C., Robichon, N., & Arenou, F. 1999, A&A, 352, 574
- Blondel, P. F. C., & Djie, H. R. E. T. A. 1994, in ASP Conf. Ser. 62, The Nature and Evolutionary Status of Herbig Ae/Be Stars, ed. P. S. Thé, M. R. Pérez, & E. P. J. van den Heuvel (San Francisco: ASP), 211
- Böhm, T., & Catala, C. 1993, A&AS, 101, 629
- Bouret, J.-C., & Catala, C. 1998, A&A, 340, 163
- Bouvier, J. 1990, AJ, 99, 946
- Cabrit, S., Edwards, S., Strom, S. E., & Strom, K. M. 1990, ApJ, 354, 687
- Calvet, N., & Gullbring, E. 1998, ApJ, 509, 802
- Camenzind, M. 1990, Rev. Mod. Astron., 3, 234
- Cardelli, J. A., Clayton, G. C., & Mathis, J. S. 1989, ApJ, 345, 245
- Carpenter, K. G., Robinson, R. D., Harper, G. M., Bennett, P. D., Brown, A., & Mullan, D. J. 1999, ApJ, 521, 382
- Chavarria-K., C., Terranegra, L., Moreno-Corral, M. A., & de Lara, E. 2000, A&AS, 145, 187
- Cohen, M., & Kuhi, L. V. 1979, ApJS, 41, 743
- Corcoran, M., & Ray, T. P. 1997, A&A, 321, 189
- de Zeeuw, P. T., Hoogerwerf, R., de Bruijne, J. H. J., Brown, A. G. A., & Blaauw, A. 1999, AJ, 117, 354
- Eiroa, C., et al. 2002, A&A, 384, 1038
- ESA. 1997, The *Hipparcos* and Tycho Catalogues (ESA SP-1200)
- Feibelman, W. A. 1995, ApJ, 443, 24
- Fiegelson, E. D., Casanova, S., Montmerle, T., & Guibert, J. 1993, ApJ, 416, 623
- Feldbrugge, P. T. M., & van Genderen, A. M. 1991, A&AS, 91, 209
- Fernandez, M., & Miranda, L. F. 1998, A&A, 332, 629
- Finkenzeller, U., & Mundt, R. 1984, A&AS, 55, 109
- Gagné, M., Caillault, J.-P., & Stauffer, J. R. 1995, ApJ, 445, 280
- Garhart, M. P., Smith, M. A., Levay, K. L., & Thompson, R. W. 1997, NASA IUE Newslett. 57
- Gauvin, L. S., & Strom, K. M. 1992, ApJ, 385, 217
- Ghandour, L., Strom, S., Edwards, S., & Hillenbrand, L. 1994, in ASP Conf. Ser. 62, The Nature and Evolutionary Status of Herbig Ae/Be Stars, ed. P. S. Thé, M. R. Pérez, & E. P. J. van den Heuvel (San Francisco: ASP), 223
- Ghez, A. M., White, R. J., & Simon, M. 1997, ApJ, 490, 353
- Gómez de Castro, A. I., & Franqueira, M. 1997, IUE-ULDA Access Guide 8:T Tauri Stars (ESA-SP 1205)
- Gregorio-Hetem, J., Lepine, J. R. D., Quast, G. R., Torres, C. A. O., & de La Reza, R. 1992, AJ, 103, 549
- Gullbring, E., Hartmann, L., Briceño, C., & Calvet, N. 1998, ApJ, 492, 323
- Hamann, F., & Persson, S. E. 1992, ApJ, 394, 628
- Hartigan, P., Edwards, S., & Ghandour, L. 1995, ApJ, 452, 736
- Hartmann, L., Avrett, E. H., Loeser, R., & Calvet, N. 1990, ApJ, 349, 168
- Hartmann, L., Hewett, R., & Calvet, N. 1994, ApJ, 426, 669
- Hartmann, L., & Kenyon, S. J. 1996, ARA&A, 34, 207
- Hartmann, L., Kenyon, S. J., & Calvet, N. 1993, ApJ, 407, 219
- Herbig, G. H. 1960, ApJS, 4, 337
- Herbig, G. H., & Bell, K. R. 1988, Third Catalog of Emission-Line Stars of the Orion Population, Lick Obs. Bull. 1111
- Herbig, G. H., & Goodrich, R. W. 1986, ApJ, 309, 294
- Herbst, W., & Shevchenko, V. S. 1999, AJ, 118, 1043
- Hillenbrand, L. A. 1997, AJ, 113, 1733
- Hillenbrand, L. A., Strom, S. E., Calvet, N., Merrill, K. M., Gatley, I., Makidon, R. B., Meyer, M. R., & Skrutskie, M. F. 1998, AJ, 116, 1816
- Hillenbrand, L. A., Strom, S. E., Vrba, F. J., & Keene, J. 1992, ApJ, 397, 613
- Huélamo, N., Franqueira, M., & Gómez de Castro, A. I. 2000, MNRAS, 312, 833
- Hughes, J., Hartigan, P., Krautter, J., & Kelemen, J. 1994, AJ, 108, 1071
- Imhoff, C. L., & Appenzeller, I. 1987, ASSL Vol. 129: Exploring the Universe with the *IUE* Satellite, ed. Y. Kondo (Dordrecht: Reidel), 295
- Johns-Krull, C. M., & Valenti, J. A. 2001, ApJ, 561, 1060
- Johns-Krull, C. M., Valenti, J. A., & Linsky, J. L. 2000, ApJ, 539, 815 (Paper II)
- Kenyon, S. J., & Hartmann, L. 1995, ApJS, 101, 117
- Kenyon, S. J., Hartmann, L., & Hewett, R. 1988, ApJ, 325, 231
- Königl, A. 1991, ApJ, 370, L39
- Lamzin, S. A. 1995, A&A, 295, L20
- . 1998, Astron. Rep., 42, 322
- Lee, T. A. 1968, ApJ, 152, 913
- Levraut, R. M. 1988, ApJ, 330, 897
- Li, J. Z., & Hu, J. Y. 1998, A&AS, 132, 173
- Liu, M. C., et al. 1996, ApJ, 461, 334
- Luhman, K. L. 2001, ApJ, 560, 287
- Malfait, K., Bogaert, E., & Waelkens, C. 1998, A&A, 331, 211
- Martin, E. L., Rebolo, R., Magazzù, A., & Pavlenko, Ya. V. 1994, A&A, 282, 503
- Massa, D., & Fitzpatrick, E. L. 2000, ApJS, 126, 517
- Meeus, G., Waelkens, C., & Malfait, K. 1998, A&A, 329, 131
- Muzerolle, J., Calvet, N., Briceño, C., Hartmann, L., & Hillenbrand, L. 2000, ApJ, 535, L47
- Muzerolle, J., Calvet, N., & Hartmann, L. 1998, ApJ, 492, 743
- . 2001, ApJ, 550, 944
- Neckel, Th., Klare, G., & Sarcander, M. 1980, A&AS, 42, 251
- Nichols, J. S., Garhart, M. P., De La Peña, M. D., & Levay, K. 1994, NASA IUE Newslett. 53
- Nichols, J. S., & Linsky, J. L. 1996, AJ, 111, 517
- O'Dell, C. R., & Wen, Z. 1994, ApJ, 436, 194
- Paatz, G., & Camenzind, M. 1996, A&A, 308, 77
- Panek, R. J. 1983, ApJ, 270, 169
- Pravdo, S. H., & Angelini, L. 1993, ApJ, 407, 232
- Reipurth, B., Pedrosa, A., & Lago, M. T. V. T. 1996, A&AS, 120, 229
- Rodríguez-Pascual, P. M., González-Riestra, R., Schartel, N., & Wamsteker, W. 1999, A&AS, 139, 183
- Rydgren, A. E., & Vrba, F. J. 1984, AJ, 89, 399
- Shu, F., Najita, J., Ostriker, E., Wilkin, F., Ruden, S., & Lizano, S. 1994, ApJ, 429, 781
- Skinner, S. L., Brown, A., & Walter, F. M. 1991, AJ, 102, 1742
- Stassun, K. G., Mathieu, R. D., Vrba, F. J., Mazeh, T., & Henden, A. 2001, AJ, 121, 1003
- Strom, K. M., Strom, S. E., Edwards, S., Cabrit, S., & Skrutskie, M. F. 1989, AJ, 97, 1451
- Strom, K. M., et al. 1990, ApJ, 362, 168
- Thé, P. S., de Winter, D., & Pérez, M. R. 1994, A&AS, 104, 315
- Thé, P. S., Pérez, M. R., Voshchinnikov, N. V., & van den Ancker, M. E. 1996, A&A, 314, 233
- Uchida, Y., & Shibata, K. 1984, PASJ, 36, 105
- Valenti, J. A., Basri, G., & Johns, C. M. 1993, AJ, 106, 2024
- Valenti, J. A., Johns-Krull, C. M., & Linsky, J. L. 2000, ApJS, 129, 399 (Paper I)
- Walter, F. M. 1986, ApJ, 306, 573
- Walter, F. M., Brown, A., Mathieu, R. D., Myers, P. C., & Vrba, F. J. 1988, AJ, 96, 297
- Walter, F. M., Vrba, F. J., Mathieu, R. D., Brown, A., & Myers, P. C. 1994, AJ, 107, 692
- Walter, F. M., et al. 1987, ApJ, 314, 297
- Waters, L. B. F. M., & Waelkens, C. 1998, ARA&A, 36, 233
- White, R. J., & Ghez, A. M. 2001, ApJ, 556, 265
- Wiese, W. L., Fuhr, J. R., & Deters, T. M., eds. 1996, Atomic Transition Probabilities of Carbon, Nitrogen, and Oxygen: A Critical Data Compilation (Washington: Am. Chem. Soc.)